DISCRETE ORDINATES TREATMENT

OF A SMALL SUBCRITICAL ASSEMBLY

A Thesis

Submitted to the Graduate Faculty of the
Louisiana State University and
Agricultural and Mechanical College
in partial fulfillment of the
requirements for the degree of

Master of Science

in

The Department of Nuclear Engineering

by

Edward James Landry
B.S., Louisiana State University, 1970

August, 1972

DEDICATED TO

my wife, Mary Gay

ACKNOWLEDGMENT

TABLE OF CONTENTS

TABLE OF CONTENTS

PAGE

v

LIST OF TABLES

LIST OF FIGURES

ABSTRACT

The discrete ordinates method of solution to the transport equation is applied to the problem of characterizing a small light-water, natural-uranium subcritical assembly. The uranium rods are 20.8 cm tall and are arranged in a hexagonal lattice 1.875 in. apart. The fuel-moderator assembly is housed in a shortened 55-gallon oil drum and mounted on a base equipped with casters.

The calculation of the neutron flux is performed with the multipurpose DOT-II (Discrete Ordinates Transport) computer code, which can be used to treat a variety of radiation transport problems. As a result of this work, the code is now operable on the LSU IBM 360/65 system.

An experimental determination of the thermal (energy less than about 0.1 ev) neutron flux was accomplished with a BF_3 detector. The general shape of the fluxes compare favorably with the calculated ones, but there is a significant difference in the magnitude of the calculated values at large radial distances. Since the DOT results are less than the measured data, a possible explanation for this discrepancy is the inadequacy of the two-dimensional treatment of the subcritical system. The computer model approximates the hexagonal fuel rings by cylindrical shells which possess a significantly higher surface area than that of the corresponding rings. This increase of surface area causes an increase in the resonance capture of the neutrons, resulting in the decrease in the flux at large radii in the computer model. The cross section data and neutron energy structure lacks detail, which could also possibly explain some of the discrepancies in the results.

Although the results of the DOT treatment to the subcritical
assembly are not highly successful, the code is a powerful one, and it
should prove to be valuable to several projects of interest at the
Nuclear Science Center. The small subcritical assembly that was con-
structed is a useful tool for education and research.

INTRODUCTION*

Over the past three decades, many methods of solving problems involving particle transport have been developed, stimulated by the development of nuclear reactors. The design and operation of these reactors depend upon a knowledge of the neutron and gamma fluxes within the system. Core specifications and shielding requirements are available primarily through approximate solutions of the Boltzmann transport equation. Exact solutions in all but the simplest cases are impossible due to the complexity of the problem.

Early attempts to solve the transport equation relied heavily on mathematical expansions and other analytical techniques. Some of the methods developed at that time, such as ordinary diffusion theory and the spherical harmonics method, are still quite useful today. With the advent of fast electronic digital computers, several new techniques, such as the original S_n difference method and the "Monte Carlo" statistical approach, came into existence. The discrete ordinates (or discrete S_n) method was introduced in 1958 after flux distortions in reactor calculations were noticed while using the earlier S_n methods. Since then, many discrete ordinates codes have appeared. One of the most recent, DOT-II (Discrete Ordinates Transport), was made available in 1969.

---

*The material discussed in this Section is obtained in part from "A Review of the Discrete Ordinates S_n Method for Radiation Transport Calculations", D. K. Trubey and Betty Maskewitz, editors, from "The Discrete S_n Approximation to Transport Theory", by Clarence E. Lee, and from "Development of Two-Dimensional Discrete Ordinates Transport Theory for Radiation Shielding", by Mynatt, Muckenthaler, and Stevens.

A description of the theory underlying the discrete ordinates method is included in this work. A simple case of monoenergetic neutrons in plane geometry is discussed first. The added complexity encountered in going to a curved medium is illustrated by considering spherical geometry. Finally, the method of treating a two-dimensional cylindrical-geometry problem is outlined.

The DOT computer code is a powerful, general-purpose code which solves the linear, energy-dependent, Boltzmann transport equation for two-dimentional geometries. The general-purpose nature of the code was instrumental in its selection to treat the problem under investigation - the characterization of a small subcritical assembly. Such a code made operable on the Louisiana State University digital computer, an IBM Systems 360 Model 65, should prove invaluable for generating solutions to many other problems in radiation transport and shielding.

The subcritical assembly under investigation is a light-water moderated, natural-uranium assembly contained within a shortened 55-gallon oil drum. Such features as its movability and the use of fuel elements that are internally and externally moderated make the system an attractive experimental and educational tool for nuclear engineering studies. The thermal neutron distribution in the assembly was experimentally determined so that a comparison could be made with the predictions of the DOT code.

Included in the appendix is a section containing useful suggestions on running the DOT code, as well as changes and corrections that must be made in the basic code package before it can be made operable on the LSU IBM 360/65.

CHAPTER I

AN OUTLINE OF TRANSPORT THEORY

The use of simple diffusion theory to describe neutron motion in a reactor is adequate for preliminary estimates of reactor design problems. Modification of the theory by the introduction of the transport mean free path and the extrapolation distance correct some of the defects of diffusion theory. However, when there is need for accurate flux data at a boundary, or when the reactor problem involves strong absorption or proximity to a neutron source, one needs the more accurate description provided by transport theory[1]. The transport theory treatment takes into account the instantaneous velocity vectors of all the neutrons contained in a given volume element. In this way, the neutron distribution is characterized more completely than it is by the use of the scalar flux, as is the case in diffusion theory.

Transport theory is based upon the Boltzmann integro-differential equation, a neutron balance equation which considers the flows in and out of a volume element within a differential solid angle in space. One form of the Boltzmann equation is:

$$\vec{\nabla}\Phi(\vec{r},\vec{\Omega},E) + \Sigma(\vec{\Omega},E)\Phi(\vec{r},\vec{\Omega},E) = \int_{\vec{\Omega}'} N\sigma_s(E,\vec{\Omega},\vec{\Omega}')\Phi(r,\vec{\Omega}',E)d\vec{\Omega}'$$
$$+ S(\vec{r},\vec{\Omega},E) \qquad (1\text{-}1)$$

The first term is the leakage term, which corresponds to the net flow of neutrons through the volume element in the direction of interest. The second term considers both absorption of neutrons and scattering-out of neutrons (in the same volume element and direction) since

$$\Sigma = \Sigma_a + \Sigma_s. \qquad (1\text{-}2)$$

The last term is the source term, which corresponds to the number of source neutrons emitted in the volume element in the direction of interest. The third term in the transport equation is the scattering-in term. It is the integral over all angular space of neutrons which initially have a direction $\vec{\Omega}'$ before scattering and $\vec{\Omega}$ after scattering. The differential microscopic cross section for scattering, σ_s, is the probability per nucleus of scattering from $\vec{\Omega}'$ to $\vec{\Omega}$.

Solution of the transport equation provides a description of the distribution in space, energy, direction, and time of the neutrons in the system. Since the dependence of cross sections on energy is so complicated, and geometrical arrangement of materials in a reactor is so complex, the transport equation cannot be solved exactly except in the simplest cases.

The most common procedure in handling the Boltzmann equation involves the expansion of the angular distribution of the neutron flux (i.e., the dependence of Φ on the direction $\vec{\Omega}$) in a complete set of orthogonal functions, namely, the Legendre polynomials in simple geometries and the spherical harmonics in general [2]. For example, in the case of monoenergetic neutrons in slab geometry, the expansion would be

$$\Phi(Z,\mu) = \sum_{\ell=0}^{\infty} \frac{2\ell+1}{4\pi} \phi_\ell(Z) P_\ell(\mu). \qquad (1\text{-}3)$$

By using the orthogonality of these polynomials, that is,

$$\int_{-1}^{1} P_\ell(\mu) P_m(\mu) d\mu = 0 \quad \text{if} \quad m \neq \ell$$

$$= \frac{2}{2\ell+1} \quad \text{if} \quad m = \ell, \qquad (1\text{-}4)$$

The integro-differential equation (1-1) is transformed into a set of differential equations from which the expansion coefficients ϕ_i can be obtained. The P_1 approximation results from retaining only the first two terms in the Legendre expansion ($n = 0, 1$), and the equations that need to be considered are

$$\frac{d\phi_1}{dx} + \sigma_0(x)\phi_0(x) = S_0(x),$$
(1-5)

and

$$\frac{d\phi_0}{dx} + 3\sigma_1(x)\phi_1(x) = 3S_1(x),$$
(1-6)

in which the ϕ_i's, σ_i's and the S_i's are the expansion coefficients in the Legendre expansion of Φ, σ_s, and S, respectively. The first two coefficients in the Legendre expansion of the angular flux have the following physical meaning: the first, ϕ_0, is the scalar flux ϕ, and the second, ϕ_1 is the neutron current J. If the source is isotropic, $S_1 = 0$ and equation (1-6) becomes a form of Fick's law, namely

$$J(x) = -D(x) \frac{d\phi(x)}{dx}$$
(1-7)

with $D = \frac{1}{3\sigma_1}$. The result may be combined with equation (1-5) to give a diffusion equation

$$-\frac{d}{dx}[D(x)\frac{d\phi(x)}{dx}] + \sigma_0(x)\phi(x) = S_0(x).$$
(1-8)

Thus, diffusion theory is an asymptotic form of transport theory which holds in regions away from boundaries and sources, where the angular distribution of neutron velocity vectors is, in fact, nearly isotropic[3].

Although the P_1 and diffusion approximations are commonly used in reactor calculations because of their simplicity, other higher

order approximations (P_3, P_5, etc.) are sometimes used when more accurate results are desired.

CHAPTER II

DISCRETE ORDINATES METHOD

The use of discrete ordinates in transport theory was first suggested by G. C. Wick in 1943[4], but the more extensive development of the method was carried out by S. Chandrasekhar in the following years[5,6]. Their early work was limited primarily to such simple problems as the transport of monoenergetic neutrons in one-dimensional slabs with isotropic scattering. The discrete ordinates (S_n) method, which is also known as the second version of the S_n method, was first introduced by B. G. Carlson in 1958[7]. The two-dimensional discrete ordinates method has, until recently, successfully treated only relatively easy problems such as criticality calculations for highly enriched uranium cylinders. Mynatt, Muckenthaler, and Stevens recently extended the two-dimensional discrete ordinates method in order to provide accurate calculations for deep-penetration radiation transport problems for shielding analysis[8].

The discrete ordinates and other related methods of numerically solving the energy-dependent neutron transport equation have been used extensively in reactor calculations. The basis of these methods lies in the evaluation of the angular flux in a number of discrete directions, instead of using the expansion in spherical harmonics or Legendre polynomials to eliminate the $\vec{\Omega}$ dependence. By considering enough directions, it is possible, in principle, to obtain a solution to any desired degree of accuracy. However, memory and core restrictions of the computer limit the accuracy that can be achieved in solving complex problems.

In using the discrete ordinates technique to solve practical problems, the energy variable is treated as discrete through a multi-group approximation, and a discrete space mesh is used for the spatial coordinates. Consequently, all the independent variables of the time-independent neutron transport equation, namely, space, $\vec{r}$, direction, $\vec{\Omega}$, and energy, E, are treated as discrete.

In order to present the discrete ordinates method in as clear and understandable a way as possible, it is necessary to consider first the one-speed or one-group transport equation for plane geometry. Once the basic method has been established, the complexity incurred when dealing with curved geometries will be illustrated by treating a problem in the most simple curved geometry, spherical geometry. Finally, the treatment of the multigroup problem in cylindrical r-z geometry will be presented.

A special aspect of plane geometry (or of rectangular carte-sian coordinates in general) is that the direction cosines relative to local coordinates do not change as the neutron streams, that is, moves through the medium without making any collisions. In curved geometry (in systems of spherical or cylindrical coordinates), however, the situation is different, as can be seen in Figure 1. The result is that the discrete ordinates treatment is complicated by the fact that the angular derivatives in the transport equation must be approximated. These derivatives arise because, in streaming, the direction variable of a neutron changes continuously in curved geometry.

FIGURE 1.   Change in Direction Cosine of Streaming Neutron
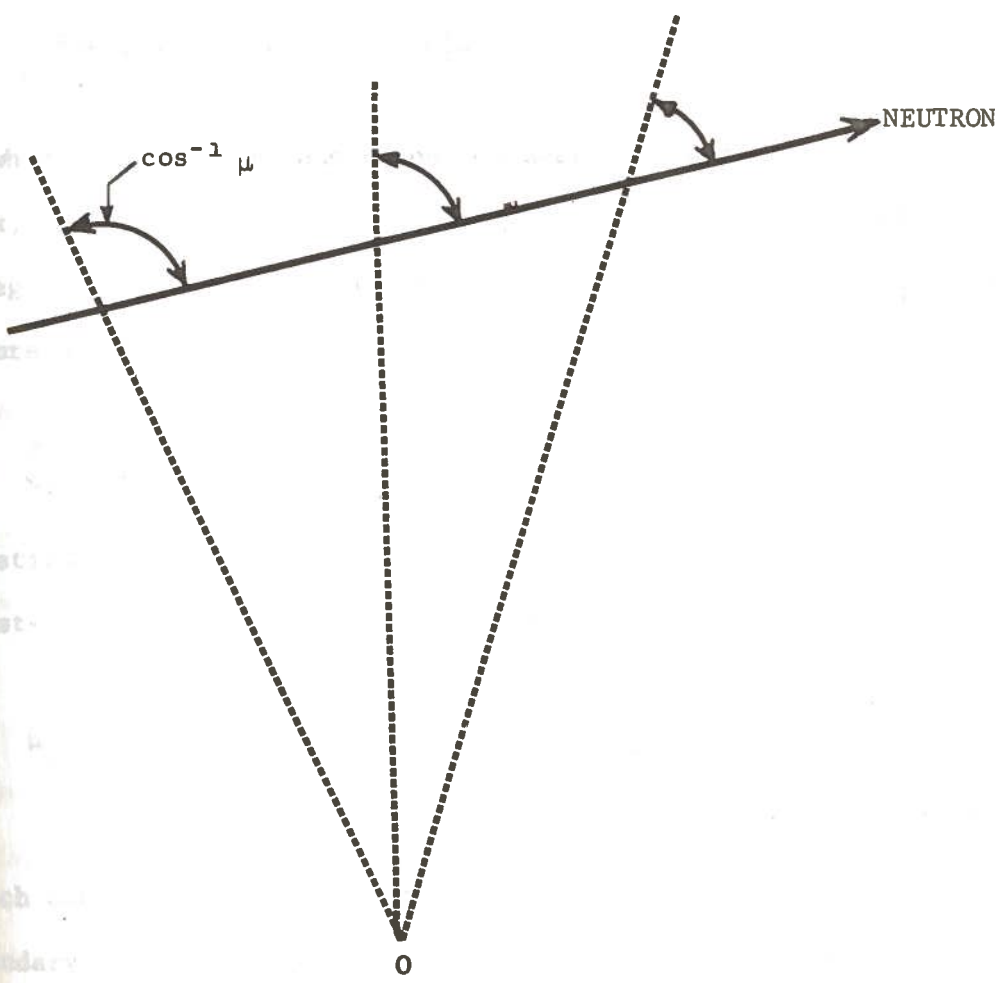
Discrete Ordinates for One Speed in Plane Geometry[9]

The one-speed transport equation in plane geometry for iso-tropic scattering and a generalized source may be written as

$$\mu \frac{\partial \Phi(x,\mu)}{\partial x} + \sigma(x)\Phi(x,\mu) = \frac{c(x)\sigma(x)}{2} \int_{-1}^{1} \Phi(x,\mu')d\mu' + Q(x,\mu), \qquad (2\text{-}1)$$

in which $c(x)$ is the mean number of neutrons emerging from a collision at x, and $\sigma(x)$ is the macroscopic cross section. Let us represent the integral by a numerical quadrature formula[*] involving $\Phi(x,\mu_i)$ with quad-rature weights (or weighting factors) w_i:

$$\int_{-1}^{1} \Phi(x,\mu')d\mu' \cong \sum_{i=1}^{N} w_i \Phi(x,\mu_i). \qquad (2\text{-}2)$$

Substitution of this into equation (2-1) yields a set of N coupled first-order differential equations for $\Phi(x,\mu_i)$:

$$\mu_j \frac{\partial \Phi(x,\mu_j)}{\partial x} + \sigma(x)\Phi(x,\mu_j) = \frac{c(x)\sigma(x)}{2} \sum_{i=1}^{N} w_i \Phi(x,\mu_i) + Q(x,\mu_j), \quad (2\text{-}3)$$

$$j = 1,2,\ldots N,$$

which can be solved readily by finite-difference techniques once the boundary conditions and character of the problem are specified.

The choice of the set of direction cosines and associated weights directly affects the accuracy achieved in solving the equations (2-3) for a given N. The set that is usually chosen is the Gauss quad-rature set which is widely used in numerical integration[10]. This set

---

[*]A quadrature formula is an approximating series, each term of which is "weighted" appropriately in order to obtain a more accurate representation.

possesses the desirable properties necessary for the chosen quadrature[11]. The cosines, μ_i's, of the Gauss quadrature are chosen to be the zeroes of the Legendre polynomials; i.e., $P_N(\mu_i) = 0$. If a unit sphere is drawn about any spatial mesh position x_i, the weights of the quadrature are that fraction of the surface area of the sphere which surrounds the intersection of the vector associated with the direction cosine and the surface of the sphere. A common set of quadrature angles for a fourth order (S_4) calculation is shown in Figure 2. In the figure, μ and η are direction cosines with respect to the x and z axes respectively, and $\xi^2 = 1 - \eta^2 - \mu^2$. Only four of the octants are shown because the geometry is identical for + or - values of ξ. In this example, all of the weights are the same, resulting in the "blocks" of the "igloo" having the same surface area. Angles 1, 4, 9, and 12 of Figure 2 are necessary for solution of the quadrature problem, but they each have zero weight associated with them[12]. The values of μ_i and w_i in the Gauss quadrature set for N = 2, 4, and 6 are presented in Table I.

TABLE I. CONSTANTS FOR THE GAUSS QUADRATURE FORMULA

N = 2: $w_1 = w_2 = 1.000$ $\mu_1 = -\mu_2 = 0.57735$

N = 4: $w_1 = w_4 = 0.65215$ $\mu_1 = -\mu_4 = 0.33998$
            $w_2 = w_3 = 0.34785$ $\mu_2 = -\mu_3 = 0.86114$

N = 6: $w_1 = w_6 = 0.46791$ $\mu_1 = -\mu_6 = 0.23862$
            $w_2 = w_5 = 0.36076$ $\mu_2 = -\mu_5 = 0.66121$
            $w_3 = w_4 = 0.17132$ $\mu_3 = -\mu_4 = 0.93247$

For anisotropic scattering, the treatment is somewhat different. Let the right side of equation (2-1) be represented by $q(x,\mu)$ so
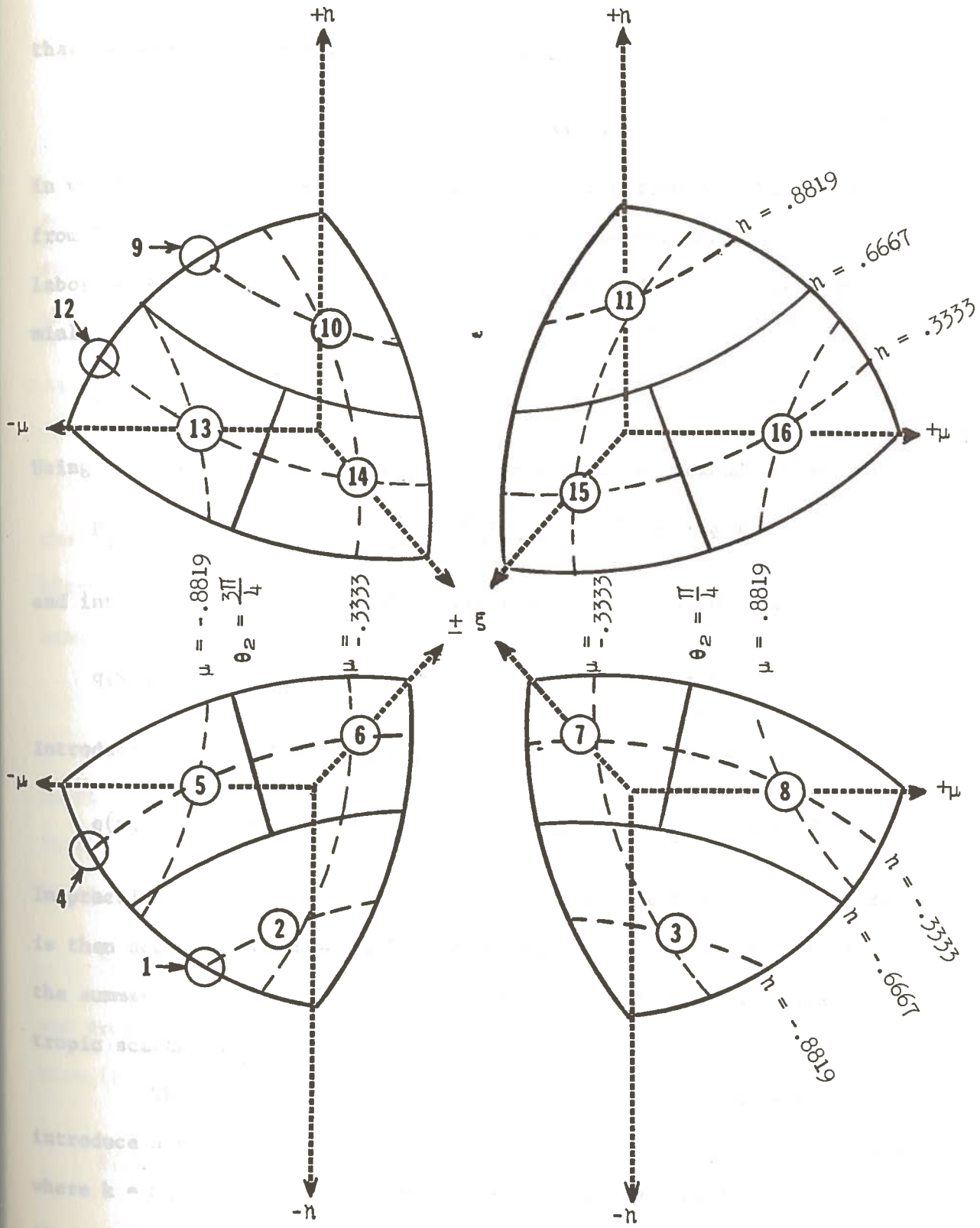
FIGURE 2. Symmetric S_4 Quadrants on Unit Sphere[12]

that (assuming scattering depends only on μ_0)

$$q(x,\mu) = c(x)\int \sigma f(x,\mu_0)\Phi(x,\mu')d\vec{\Omega}' + Q(x,\mu), \qquad (2\text{-}4)$$

in which $f(x,\mu_0)$ is the transfer probability function for scattering from $\vec{\Omega}'$ to $\vec{\Omega}$, and μ_0 is the cosine of the scattering angle in the laboratory system (i.e., $\vec{\Omega}'\cdot\vec{\Omega} = \mu_0$). Expanding σf in Legendre polynomials:

$$\sigma f = \sum_{\ell=0}^{\infty} \frac{2\ell+1}{4\pi} \sigma_\ell P_\ell(\mu_0). \qquad (2\text{-}5)$$

Using the functional relationship of the associated Legendre polynomials,

$$P_\ell(\mu_0) = P_\ell(\mu)P_\ell(\mu') + 2\sum_{m=1}^{\ell} \frac{(\ell-m)!}{(\ell+m)!}P_\ell^m(\mu)P_\ell^m(\mu')\cos m(\phi-\phi'), \qquad (2\text{-}6)$$

and integrating over azimuthal angles (multiplying by 2π) gives

$$q(x,\mu) = \frac{c(x)}{2}\sum_{\ell=0}^{\infty}(2\ell+1)\sigma_\ell P_\ell(\mu)\int_{-1}^{1}P_\ell(\mu')\Phi(x,\mu')d\mu' + Q(x,\mu). \qquad (2\text{-}7)$$

Introducing the quadrature (2-2) into equation (2-7) yields

$$q(x,\mu_j) = \frac{c(x)}{2}\sum_{\ell=0}^{\infty}(2\ell+1)\sigma_\ell P_\ell(\mu_j)\sum_{i=1}^{N}w_i P_\ell(\mu_i)\Phi(x,\mu_i) + Q(x,\mu_j). \qquad (2\text{-}8)$$

In practice, the sum over ℓ will be cut off at some finite value L; it is then necessary to specify L cross sections, σ_ℓ, in order to perform the summation. Otherwise, the procedure is identical to that for iso-tropic scattering.

The first step in solving the system of equations (2-3) is to introduce a space mesh, i.e., a set of discrete values of x, namely x_k, where k = 0, 1, 2,...,K, such that the left boundary of the system is at x_0 and the right boundary at x_K. Points are usually chosen to lie on interfaces if present. The derivative terms can then be approximated

by finite differences:

$$\frac{\partial \Phi(x,\mu_j)}{\partial x} \bigg|_{x=x_{k+\frac{1}{2}}} \cong \frac{\Phi(x_{k+1},\mu_j)-\Phi(x_k,\mu_j)}{x_{k+1}-x_k} , \qquad (2\text{-}9)$$

specifying that $x_{k+\frac{1}{2}} = \frac{1}{2}(x_k + x_{k+1})$. Again representing the right-hand side of equation (2-3) by $q(x,\mu_j)$ to allow for anisotropic scattering, this equation at the point $x_{k+\frac{1}{2}}$ becomes

$$\mu_j \frac{\Phi(x_{k+1},\mu_j)-\Phi(x_k,\mu_j)}{x_{k+1}-x_k} + \sigma(x_{k+\frac{1}{2}})\Phi(x_{k+\frac{1}{2}},\mu_j) = q(x_{k+\frac{1}{2}},\mu_j). \qquad (2\text{-}10)$$

The method of solution is by iteration. Assume, first of all, that $q(x,\mu_j)$ is known; a value is estimated the first time and there-after it is available as a result of each preceding iteration. We will assume the flux to be slowly varying over any mesh so that

$$\Phi(x_{k+\frac{1}{2}},\mu_j) \cong \frac{\Phi(x_k,\mu_j)+\Phi(x_{k+1},\mu_j)}{2} . \qquad (2\text{-}11)$$

Substitution of equation (2-11) into (2-10) results in an expression that can be solved for $\Phi(x_{k+1},\mu_j)$ in terms of $\Phi(x_k,\mu_j)$, or _vice_ _versa_. Letting

$$\Delta_{k+\frac{1}{2}} \equiv x_{k+1} - x_k,$$

and dropping the arguments of quantities at $x_{k+\frac{1}{2}}$, it is found from equation (2-10) that

$$\Phi(x_{k+1},\mu_j) = \frac{1-\frac{\sigma\Delta}{2\mu_j}}{1+\frac{\sigma\Delta}{2\mu_j}} \Phi(x_k,\mu_j) + q\frac{\Delta}{\mu_j(1+\frac{\sigma\Delta}{2\mu_j})} , \qquad (2\text{-}12)$$

and

$$\Phi(x_k,\mu_j) = \frac{1+\frac{\sigma\Delta}{2\mu_j}}{1-\frac{\sigma\Delta}{2\mu_j}} \Phi(x_{k+1},\mu_j) - q \frac{\Delta}{\mu_j(1-\frac{\sigma\Delta}{2\mu_j})} . \qquad (2\text{-}13)$$

With vacuum boundary conditions, $\Phi(x_o,\mu_j)$ is zero for all posi-
tive μ_j; hence, $\Phi(x_k,\mu_j)$ for positive μ_j can be found by repeated ap-
plication of equation (2-12). Similarly $\Phi(x_K,\mu_j)$ is zero for all nega-
tive μ_j and equation (2-13) can be applied to determine $\Phi(x_k,\mu_j)$ for
negative values of μ_j. Then, knowing $\Phi(x_{k+\frac{1}{2}},\mu_j)$ from equation (2-11),
the value of q can be recalculated using equation (2-8), and the problem
solved by iteration.

If reflecting boundaries are present at $x = x_K$, then $\Phi(x_K,\mu_j)$
may be found for negative μ_j by using

$$\Phi(x_K,\mu_j) = \Phi(x_K,-\mu_j).$$

If there are reflecting boundaries at both interfaces, i.e., at x_o and
x_K, then it is possible to run a series of $\frac{1}{2}N$ problems (N = number of
directions considered), which for the nth problem the boundary condi-
tion at x_o is

$$\Phi(x_o,\mu_j) = \delta_{jn},$$

in which δ_{jn} is the Kronecker delta defined by

$$\delta_{jn} = 1 \text{ for } j = n,$$
$$\delta_{jn} = 0 \text{ for } j \neq n.$$

By taking an appropriate linear combination of these $\frac{1}{2}N$ conditions, the
reflecting boundary conditions

$$\Phi(x_o,\mu_j) = \Phi(x_o,-\mu_j)$$

can be satisfied.

Recall that equation (2-12) is to be used for positive μ_j and equation (2-13) for negative μ_j. In both cases, the coefficient of Φ on the right-hand side is less than unity. Consequently, errors in Φ, which may be introduced in the numerical approximation, are attenuated rather than amplified during the process of obtaining a solution.

Notice also that if Δ is large in comparison with $2|\mu_j|/\sigma$ the coefficients of Φ on the right side of the equations become negative. Thus if q is small, negative values of Φ are obtained, a result which is both physically and numerically undesirable. It will be seen later that computer codes correct for this phenomena to a certain extent.

As the number of angular directions, N, in equation (2-2) are increased, some of the values of μ_j, especially $\mu_{N/2}$, will become increasingly closer to zero. In order to avoid large values of $\sigma\Delta/\mu_{N/2}$, it is therefore necessary to increase simultaneously the number of space points.

Discrete Ordinates for One Speed in Curved Geometries[9]

Now that the basic method for applying discrete ordinates in the simplest case has been outlined, it becomes necessary to examine the more complex situation encountered when dealing with curved geometries. It was mentioned earlier that a problem arises in curved geometry because the angular coordinate of the neutron, in a local coordinate system, changes because of streaming. The result is a further coupling between equations describing neutron flows in discrete directions. For simplicity and clarity, spherical geometry will be considered here.

The one-speed transport equation in spherical geometry can be written as

$$\mu \frac{\partial \Phi(r,\mu)}{\partial r} + \frac{1}{r}(1-\mu^2) \frac{\partial \Phi(r,\mu)}{\partial \mu} + \sigma(r)\Phi(r,\mu) = q(r,\mu), \qquad (2\text{-}14)$$

in which $q(r,\mu)$, the source term, may include anisotropic scattering and sources. Here, the treatment of the source term is identical to that for plane geometry. In more general geometries, the only difference is that the expansion is done is spherical harmonics rather than Legendre polynomials.

The spherical harmonics are functions which are orthonormal over a spherical surface; i.e., they are orthonormal with respect to the azimuthal angle $\emptyset$ and the polar angle θ. They are defined by

$$Y_n^m(\theta,\emptyset) \equiv \sqrt{\frac{2n+1}{4\pi} \frac{(n-m)!}{(n+m)!}} \; P_n^m(\cos\theta)e^{im\emptyset},$$

in which $P_n^m(\cos\theta)$ are the associated Legendre polynomials defined by

$$P_n^m(x) = (1-x^2)^{m/2} \frac{d^m}{dx^m} P_n(x)$$

where $P_n(x)$ are the Legendre polynomials[13].

The problem in spherical geometry is how to approximate the second term in equation (2-14), especially $\partial\Phi/\partial\mu$. One solution was proposed by B. Carlson[7] in his original S_N method. The dependence of $\Phi(r,\mu)$ on μ was approximated by a series of connected straight line segments between $\mu = -1$ and $\mu = 1$, as shown in Figure 3. In one dimensional geometries, N indicates the number of segments chosen to represent the angular flux distribution. In Figure 3 the actual distribution, indicated by the broken line, is approximated by four linear segments;

FIGURE 3. Linear Segments Approximating Actual Angular Flux Distribution

$$V = 4/3\pi(r_{i+1}^3 - r_i^3).$$

In evaluating the integral over μ, one term of the quadrature formula, i.e.,

$$\int_{\mu_{n-\frac{1}{2}}}^{\mu_{n+\frac{1}{2}}} f(\mu)d\mu \approx w_n f(\mu_n),$$

has been used, and $\bar{q}$ and $\bar{\Phi}$ are the second moments of the volumetric averages over the cell, e.g.,

$$\bar{q}(r_{i+\frac{1}{2}},\mu_n) \approx \frac{4\pi}{V}\int_{r_i}^{r_{i+1}} r^2 q(r,\mu_n)dr.$$

The first term on the left of equation (2-15) can be integrated by using the same approximation for the partial μ integral to give

$$2\pi w_n \mu_n [A_{i+1}\Phi(r_{i+1},\mu_n) - A_i\Phi(r_i,\mu_n)]. \tag{2-19}$$

The second term can be integrated first over the limited range of μ, and then over the volume of the cell, which results in

$$8\pi^2 \int_{r_i}^{r_{i+1}} r[(1-\mu_{n+\frac{1}{2}}^2)\Phi(r,\mu_{n+\frac{1}{2}}) - (1-\mu_{n-\frac{1}{2}}^2)\Phi(r,\mu_{n-\frac{1}{2}})]dr. \tag{2-20}$$

This can be written simply as

$$2\pi[a_{n+\frac{1}{2}}\Phi(r_{i+\frac{1}{2}},\mu_{n+\frac{1}{2}}) - a_{n-\frac{1}{2}}\Phi(r_{i+\frac{1}{2}},\mu_{n-\frac{1}{2}})], \tag{2-21}$$

in which the coefficients $a_{n\pm\frac{1}{2}}$ are to be determined.

Combining equations (2-18), (2-19), and (2-21), the complete difference equation resulting from the integration of the one-speed transport equation over a r,μ mesh is

$$\mu_n[A_{i+1}\Phi(r_{i+1},\mu_n) - A_i\Phi(r_i,\mu_n)]$$

$$+ \frac{a_{n+\frac{1}{2}}\Phi(r_{i+\frac{1}{2}},\mu_{n+\frac{1}{2}}) - a_{n-\frac{1}{2}}\Phi(r_{i+\frac{1}{2}},\mu_{n-\frac{1}{2}})}{w_n}$$

$$= V(\bar{q}-\sigma\bar{\bar{\Phi}}). \tag{2-22}$$

A recurrence relation for the $a_{n\pm\frac{1}{2}}$'s exists for the case of an infinite medium in which the flux is constant and isotropic. In this case there is no net current, and the conservation principle requires that

$$\bar{q} = \sigma\bar{\bar{\Phi}}.$$

From equation (2-22) this requires that

$$\mu_n w_n(A_{i+1}-A_i) = -a_{n+\frac{1}{2}}+a_{n-\frac{1}{2}}. \tag{2-23}$$

Since it can be shown that $a_{\frac{1}{2}}$ is zero[2], equation (2-23) allows the determination of all values of a.

The terms in equation (2-22) can be interpreted in the following manner. When multiplied by w_n, the first two terms on the left side are the neutron flows across the areas of radii r_{i+1} and r_i in the nth μ interval. The a terms represent streaming flows which transfer neutrons from the $n-\frac{1}{2}$ direction into the n interval and from the n interval into the $n+\frac{1}{2}$ direction, respectively; the terms on the right-hand side are, of course, the source and the sink.

The one-speed transport equation (2-15) has been changed into a difference equation (2-22), which now needs to be solved. As it stands, however, equation (2-22) cannot be solved because there are too many $\Phi(r,\mu)$ values; i.e., there are too few equations for the number

of unknowns. Consequently, some further relations must be postulated.
Suppose the problem being solved is one with a boundary condition at
the outer radius, r_I. As in the case for plane geometry, some value is
assigned to $q(r,\mu)$ so that $\bar{q}$ is known. Starting at the outer boundary
with the boundary condition given as the incoming angular flux $\Phi(r,\mu)$
for $\mu < 0$, the direction $\mu = -1$ is considered. It is obvious that for
this direction the transport equation, equation (2-14), is the same as
that for plane geometry, equation (2-1). As in plane geometry, inte-
gration is performed inward to the center along this direction, so that
$\Phi(r_{i+\frac{1}{2}},\mu_{\frac{1}{2}})$ can be determined for all values of i, with $\mu_{\frac{1}{2}} = -1$.

Next, the inward integration is started for μ_1; at any step
in this process $\Phi(r_{i+\frac{1}{2}},\mu_{\frac{1}{2}})$ is known and $\Phi(r_{i+1},\mu_1)$ is obtained from
the preceding step or initially from the boundary conditions. Thus,
in equation (2-22), for n = 1, the quantities $\Phi(r_{i+\frac{1}{2}},\mu_{\frac{1}{2}})$ and $\Phi(r_{i+1},\mu_1)$
are known, but three quantities, $\Phi(r_i,\mu_1)$, $\Phi(r_{i+\frac{1}{2}},\mu_{\frac{3}{2}})$, and $\bar{\bar{\Phi}}(r_{i+\frac{1}{2}},\mu_1)$,
are still unknown. In general, for any $\mu_n < 0$, the unknown quantities
in equation (2-22) are $\Phi(r_i,\mu_n)$, $\Phi(r_{i+\frac{1}{2}},\mu_{n+\frac{1}{2}})$, and $\bar{\bar{\Phi}}(r_{i+\frac{1}{2}},\mu_n)$. As was
mentioned before, we need two additional relations between these three
quantities to solve the equation.

Many such relations have been proposed and implemented, but
there are two essential requirements: First, the equation relating
the centered flux and the two end-point fluxes should provide a good
approximation to the true variation of the flux in the neighborhood of
the cell; and second, these equations, when combined with equation (2-22),
must produce a final set of equations which may be easily and quickly
solved on the computer[8].

One simple relation, the "diamond-difference method"[14],
assumes Φ to be linear between adjacent r, μ mesh points (Figure 5);
thus,

$$2\Phi(r_{i+\frac{1}{2}}, \mu_n) \cong \Phi(r_{i+1}, \mu_n) + \Phi(r_i, \mu_n), \tag{2-24}$$

$$\cong \Phi(r_{i+\frac{1}{2}}, \mu_{n+\frac{1}{2}}) + \Phi(r_{i+\frac{1}{2}}, \mu_{n-\frac{1}{2}}). \tag{2-25}$$

Equations (2-24) and (2-25) may be used in equation (2-22) to eliminate
two unknowns, $\Phi(r_i, \mu_n)$ and $\Phi(r_{i+\frac{1}{2}}, \mu_{n+\frac{1}{2}})$. Using equation (2-23) to
write the denominator in symmetrical form, equation (2-22) can be solved
for $\bar{\Phi}(r_{i+\frac{1}{2}}, \mu_n)$ to give

$$\bar{\Phi}(r_{i+\frac{1}{2}}, \mu_n)$$

$$= \frac{-\mu_n(A_i + A_{i+1})\Phi(r_{i+1}, \mu_n) + \frac{1}{w_n}(a_{n+\frac{1}{2}} + a_{n-\frac{1}{2}})\Phi(r_{i+\frac{1}{2}}, \mu_{n-\frac{1}{2}}) + V\bar{q}}{-\mu_n(A_i + A_{i-1}) + \frac{1}{w_n}(a_{n+\frac{1}{2}} + a_{n-\frac{1}{2}}) + \sigma V} . \tag{2-26}$$

Once $\bar{\Phi}$ has been determined, by using the $\Phi(r_{i+1}, \mu_n)$ and $\Phi(r_{i+\frac{1}{2}}, \mu_{n-\frac{1}{2}})$
obtained above, equations (2-24) and (2-25) may be used to calculate
$\Phi(r_i, \mu_n)$ and $\Phi(r_{i+\frac{1}{2}}, \mu_{n+\frac{1}{2}})$, which will be required for subsequent steps.

By repeating the steps outlined above, the values of $\bar{\Phi}$ may be
found for all space points and all ingoing direction, i.e., for $\mu_n < 0$.
For outgoing directions, i.e., for $\mu_n > 0$, the method is similar except
that integration is performed outward. As a boundary or initial con-
dition, isotropy of the neutron flux at the center may be used so that

$$\Phi(o, \mu_n) = \Phi(o, -\mu_n), \tag{2-27}$$

where, for positive μ_n, the right-hand side is known from the inward
integration. Hence, $\Phi(o, \mu_n)$ is available for starting the outward
integration. In this direction, $\Phi(r_i, \mu_n)$ is known and $\Phi(r_{i+1}, \mu_n)$ is
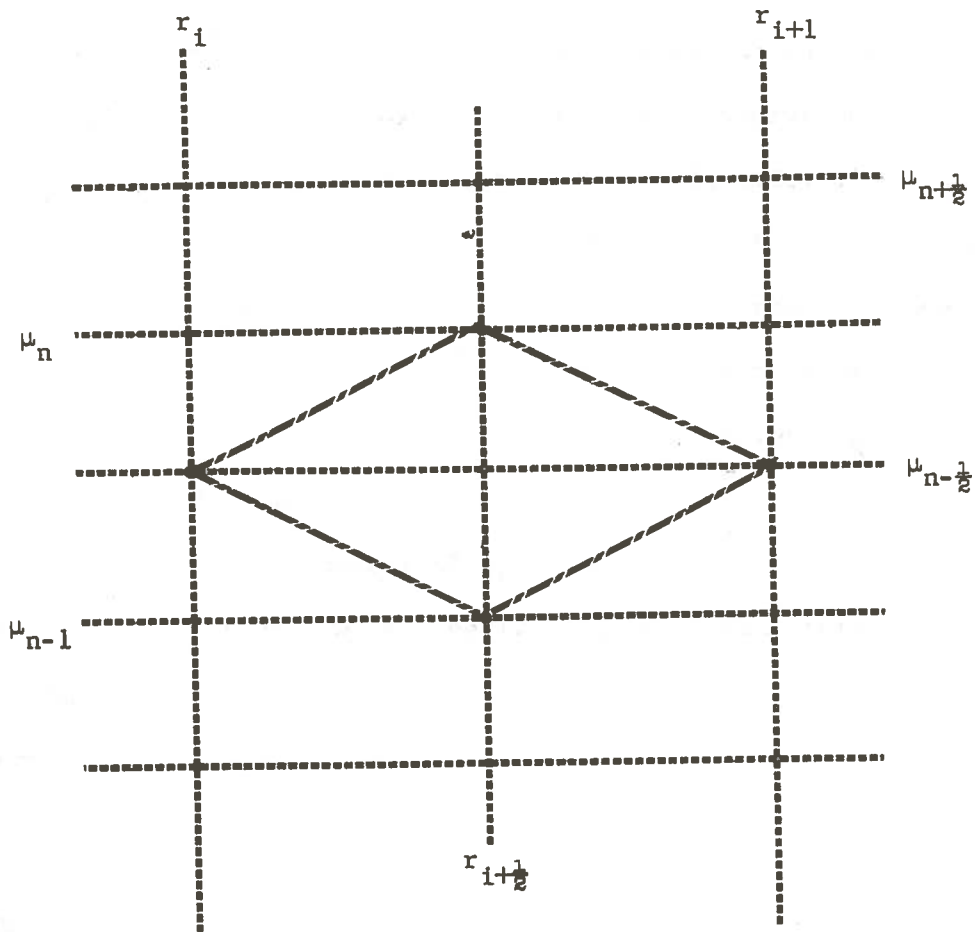
FIGURE 5. The r,μ Mesh for a "Diamond-difference" Scheme

hence, in this case N is 4. Obviously, the larger the number of direc-
tions, (N + 1), used to express the angular flux distribution, the
better the approximation.

The S_N method was used for several years and was regarded to
be quite accurate; however, flux aberrations were observed particularly
near the center of spheres. It was found that this difficulty was
caused by the use of an unsymmetric quadrature. Further shortcomings
were that the original S_N technique could not be extended to higher
dimension geometries and was limited to isotropic scattering[8].
These difficulties led to the development of the discrete S_N method,
which will now be described.

In deriving the numerical approximation to the transport
equation, a conservation law is closely followed. Each term in the
equation represents a physical component in neutron conservation, such
as absorption in the cell or flow across a face.

Equation (2-14) may be written

$$\frac{\mu}{r^2} \frac{\partial}{\partial r} (r^2 \Phi) + \frac{1}{r} \frac{\partial}{\partial \mu}[(1-\mu^2)\Phi] + \sigma \Phi = q. \tag{2-15}$$

A conservation relationship can be derived by integrating equation
(2-15) over a region in r, μ space. Thus, upon integration over a
volume from r_i to r_{i+1} (i.e., multiplication by $4\pi r^2$ and integration
over r from r_i to r_{i+1}) and over all directions (i.e., multiplication
by 2π and integration over μ from -1 to 1), the first term in equation
(2-15) becomes

$$4\pi(r_{i+1})^2 2\pi \int_{-1}^{1} \mu \Phi(r_{i+1},\mu)d\mu - 4\pi(r_i^2)2\pi \int_{-1}^{1} \mu \Phi(r_i,\mu)d\mu$$
$$= A_{i+1}J_{i+1} - A_i J_i, \tag{2-16}$$

in which $A_i = 4\pi r_i^2$ is the area of the surface of radius r_i, and

$$J_i = 2\pi \int_{-1}^{1} \mu \Phi(r_i, \mu) d\mu$$

is the outward radial current at $r = r_i$. (Subscripts i+1 have similar meanings.) The second term in equation (2-15) becomes zero after integration; hence, the net result is

$$A_{i+1}J_{i+1} - A_i J_i = 8\pi^2 \int_{r_i}^{r_{i+1}} r^2 dr \int_{-1}^{1} (q - \sigma\Phi) d\mu, \tag{2-17}$$

$$= \text{source} - \text{sink},$$

since the q term represents the neutron source and $\sigma\Phi$ the neutrons lost in various collisions. Thus, a conservation relationship is established.

The foregoing procedure will now be followed, except that the integration will be over a limited range of μ rather than from -1 to 1. Figure 4 illustrates a r,μ mesh in which the $\{r_i\}$ are points on boundaries between regions and the cross sections are assumed to be constant within an interval r_i, r_{i+1}; the points μ_n are selected to coincide with the μ values in the quadrature formula of equation (2-2).

Consider a typical cell bounded by r_i, r_{i+1} and by $\mu_{n-\frac{1}{2}}$, $\mu_{n+\frac{1}{2}}$, as shown in Figure 4. If equation (2-15) were integrated over the volume of the cell and over a segment of μ between $\mu_{n-\frac{1}{2}}$ and $\mu_{n+\frac{1}{2}}$, then the source (q) minus collision ($\sigma\Phi$) terms become

$$8\pi^2 \int_{r_i}^{r_{i+1}} r^2 dr \int_{\mu_{n-\frac{1}{2}}}^{\mu_{n+\frac{1}{2}}} [q(r,\mu) - \sigma\Phi(r,\mu)] d\mu$$

$$\approx 8\pi^2 w_n \int_{r_i}^{r_{i+1}} r^2 [q(r,\mu_n) - \sigma\Phi(r,\mu_n)] dr$$

$$= 2\pi w_n V[\bar{q}(r_{i+\frac{1}{2}}, \mu_n) - \sigma\bar{\Phi}(r_{i+\frac{1}{2}}, \mu_n)], \tag{2-18}$$

in which V is the volume of the spherical shell between r_i and r_{i+1}:
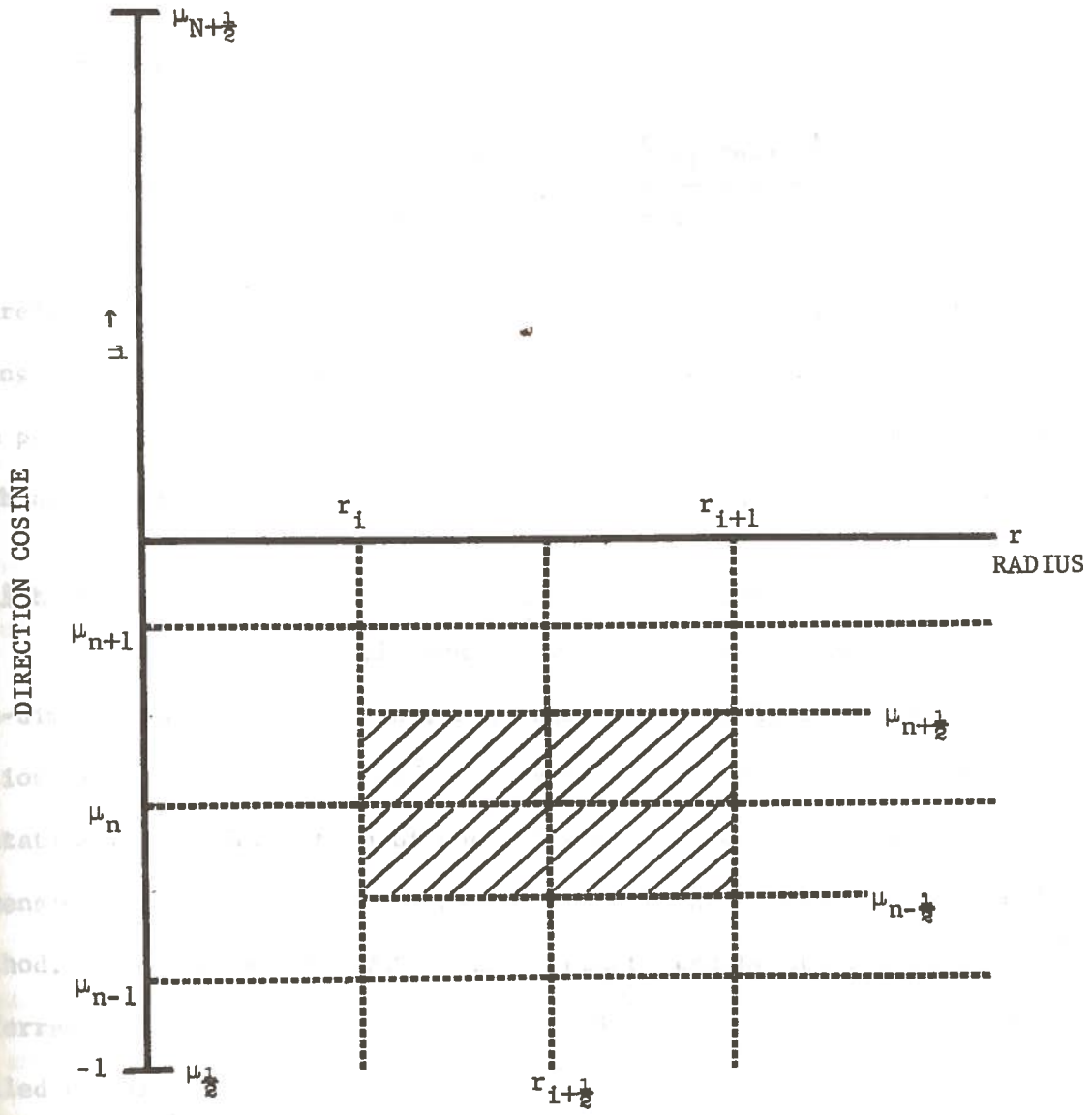
FIGURE 4. Portion of a r,μ Mesh

21

unknown so that instead of equation (2-26) we have

$$\bar{\bar{\Phi}}(r_{i+\frac{1}{2}},\mu_n)$$

$$= \frac{\mu_n(A_i+A_{i+1})\bar{\Phi}(r_i,\mu_n) + \frac{1}{w_n}(a_{n+\frac{1}{2}}+a_{n-\frac{1}{2}})\bar{\Phi}(r_{i+\frac{1}{2}},\mu_{n-\frac{1}{2}}) + V\bar{q}}{\mu_n(A_i+A_{i+1}) + \frac{1}{w_n}(a_{n+\frac{1}{2}}+a_{n-\frac{1}{2}}) + \sigma V}. \quad (2-28)$$

Therefore $\bar{\bar{\Phi}}$ can be found for all angles μ_n and all space points $r_{i+\frac{1}{2}}$. Using these calculated values, a new value for $\bar{q}$ can be computed and the process repeated until convergence is reached. There are techniques, such as the method of scaling, by which convergence can be accelerated[15].

Multigroup Discrete Ordinates for Cylindrical r-z Geometry[8]

The previous development of the discrete ordinates method for one-dimensional plane and spherical geometries facilitates the presentation of the multigroup problem in cylindrical r-z geometry. The presentation of the derivation of the difference equations for this two-dimensional geometry is, of necessity, merely an outline of the actual method. The rigorous derivation is somewhat lengthy and the reader is referred to the work by Mynatt, Muckenthaler, and Stevens[8] for a detailed explanation of the steps.

The derivation of the difference equation (corresponding to equation (2-22) for spherical geometry) is accomplished in a term-wise consistent manner directly from the energy-dependent, cylindrical geometry form of the transport equation

$$\frac{d\Phi(r,z,\theta,\hbar,\psi,E)}{ds} + \sigma(r,z,\theta,E)\Phi(r,z,\theta,\hbar,\psi,E) = S(r,z,\theta,\hbar,\psi,E)$$

$$+ \int_{-1}^{+1}\int_0^{2\pi}\int_0^\infty \sigma_s(r,z,\theta;E',\vec{\Omega}'\to E,\vec{\Omega})\Phi(r,z,\theta,\hbar',\psi',E')dE'd\psi'd\hbar'. \quad (2-29)$$

The coordinate system for cylindrical geometry is shown in Figure 6. As can be seen, ψ is the azimuthal angle, and $\hbar$ and μ define the location of the neutron direction vector $\vec{\Omega}$ with respect to $\hat{z}$ and $\hat{r}$, respectively.

Using Figure 6, $d\Phi/ds$ can be expressed as derivatives of the various spatial and angular coordinates. Defining

$$\Phi(P) \equiv \Phi(r,z,\theta,\hbar,\psi,E),$$
$$\Phi(P') \equiv \Phi(r,z,\theta,\hbar',\psi',E'),$$

$$(2\text{-}30)$$

and noting that for two-dimensional r-z geometry, the material composition and geometry are invariant with respect to θ, equation (2-29) becomes

$$\mu\,\frac{\partial\Phi(P)}{\partial r} + \hbar\,\frac{\partial\Phi(P)}{\partial(z)} - \frac{\xi}{r}\,\frac{\partial\Phi(P)}{\partial\psi} + \sigma(r,z,E)\Phi(P) = S(P)$$
$$+ \int_{-1}^{+1}\int_{o}^{2\pi}\int_{o}^{\infty} \sigma_s(r,z;E',\vec{\Omega}'\to E,\vec{\Omega})\Phi(P')dE'd\psi'd\hbar'. \qquad (2\text{-}31)$$

In the derivation of the difference equations for the one-speed spherical geometry case, integration was performed over the volume of an r,μ mesh cell and over a limited range of μ. In an analagous manner, the difference equations here will be derived by integrating equation (2-31) over a finite difference cell. Since we are dealing with the energy-dependent transport equation, the differential cell will be a phase space cell given by

$$dP = 2\pi r\ dr\ dz\ d\hbar\ d\psi\ dE. \qquad (2\text{-}32)$$

The finite difference phase space cell, ΔP, results from integrating equation (2-32) over a five-dimensional finite cell
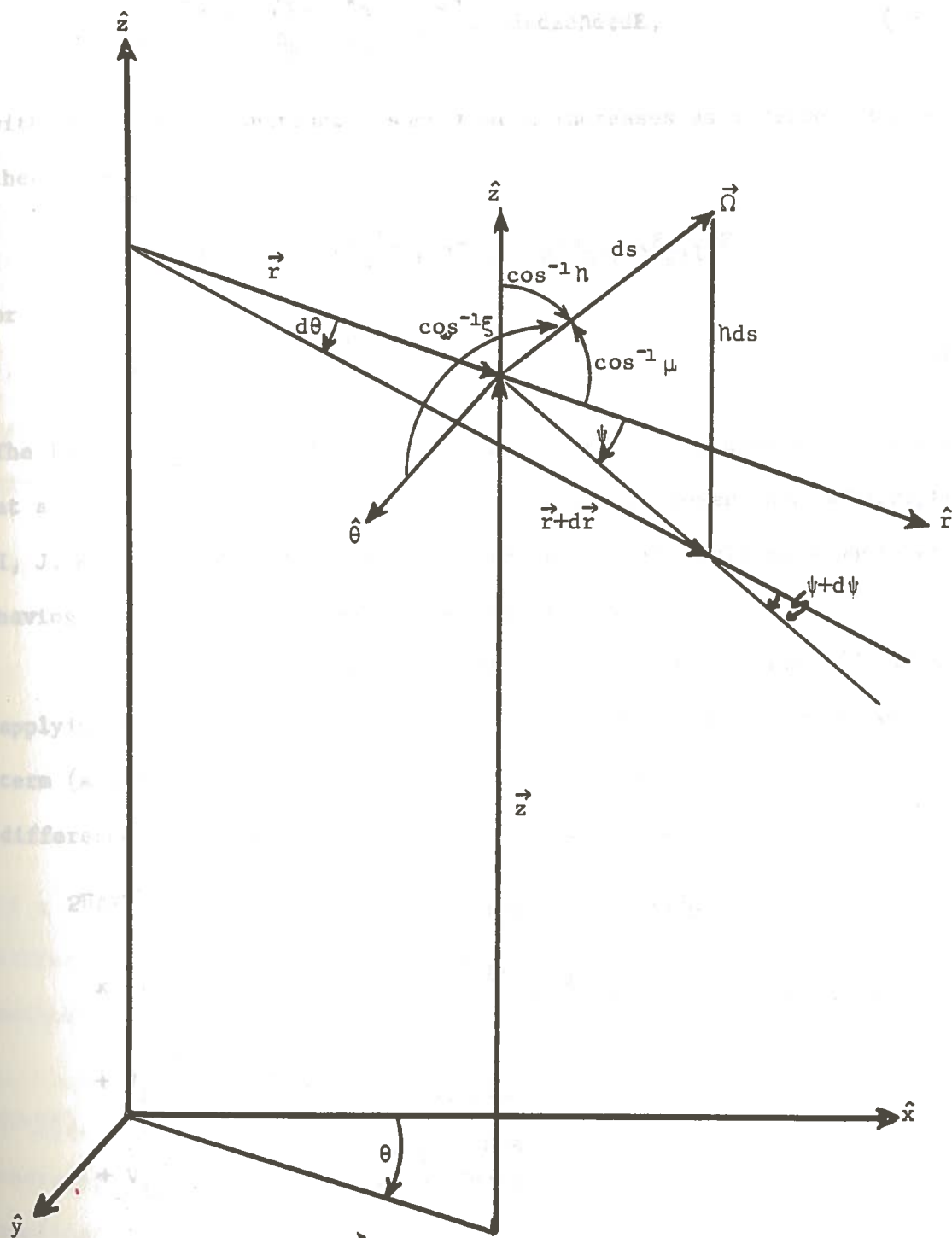
FIGURE 6. The Coordinate System for Cylindrical Geometry

$$\Delta P = \int_{r_i}^{r_{i+1}} \int_{z_j}^{z_{j+1}} \int_{\eta_k}^{\eta_{k+1}} \int_{\psi_{n+1}}^{\psi_n} \int_{E_g}^{E_{g+1}} 2\pi r \, dr \, dz \, d\eta \, d\psi \, dE, \tag{2-33}$$

with the ψ_n mesh constructed such that n increases as ψ decreases. We then have

$$\Delta P = \pi(r_{i+1}^2 - r_i^2)(z_{j+1} - z_j)(\eta_{k+1} - \eta_k)(\psi_n - \psi_{n+1})(E_{g+1} - E_g),$$

or

$$\Delta P = V_{I,J} \Delta \eta_K \Delta \psi_N \Delta E_G. \tag{2-34}$$

The lower case subscripts, i, j, k, n, g, refer to a quantity evaluated at a surface of the finite phase space cell, and upper case subscripts, I, J, K, N, G, refer to quantities defined for the cell as a whole or having been averaged or integrated over the cell.

Upon integrating each of the six terms in equation (2-31) by applying the integral operator (2-33) in a consistent manner to each term (a very tedious process), the result is the discrete ordinates difference equation for cylindrical r-z geometry:

$$2\pi \Delta z_j \bar{\mu}_D (r_{i+1} \Phi_{G,i+1,J,D} - r_i \Phi_{G,i,J,D}) + 2\pi \bar{r}_I \Delta r_I \bar{\bar{\eta}}_D$$

$$x \; (\Phi_{G,I,j+1,D} - \Phi_{G,I,j,D}) + \frac{\Delta z_j}{w_D}(\gamma_{n+1} \Phi_{G,I,J,n+1,K} - \gamma_n \Phi_{G,I,J,n,K})$$

$$+ V_{I,J} \Sigma_G^T \Phi_{G,I,J,D} = V_{I,J} S_{G,I,J,D}$$

$$+ V_{I,J} \sum_{\ell=0}^{LMAX} \sum_{m=0}^{\ell} A_D^{\ell,m} \sum_{G'=1}^{G} S_{G,G'}^{\ell,m} \sum_{D'=1}^{NOA} A_{D'}^{\ell,m} \Phi_{G',I,J,D'} w_{D'} \tag{2-35}$$

The relationships between the mean angles denoted by subscript D and the angle end points (n,K,) and (n+1,K) is clarified in the discussion of the space-angle mesh sweep. The curvature coefficients, γ_n, are defined by

$$\gamma_n \equiv \tfrac{1}{2}\Delta r_I \Delta n_K \xi_n = \tfrac{1}{2}\Delta r_I \Delta n_K \sqrt{1-n_K^2}\sin\psi_n. \qquad (2\text{-}36)$$

The last term of equation (2-35) is derived from the scattering integral in the transport equation (2-31). During the derivation, the scattering cross section was expanded in Legendre polynomials, and the energy integral was replaced by a sum of group integrals.

Just as in the case of spherical geometry, supplementary difference equations must be combined with equation (2-35) in order to obtain a solution. A possible set of additional difference equations is given by

$$\Phi_{G,I,J,D} = a\Phi_{G,i+1,J,D} + (1-a)\Phi_{G,i,J,D}, \ \mu > 0; \qquad (2\text{-}37)$$

$$\Phi_{G,I,J,D} = (1-a)\Phi_{G,i+1,J,D} + a\Phi_{G,i,J,D}, \ \mu < 0; \qquad (2\text{-}38)$$

$$\Phi_{G,I,J,D} = b\Phi_{G,I,j+1,D} + (1-b)\Phi_{G,I,j,D}, \ n > 0; \qquad (2\text{-}39)$$

$$\Phi_{G,I,J,D} = (1-b)\Phi_{G,I,j+1,D} + b\Phi_{G,I,j,D}, \ n < 0; \qquad (2\text{-}40)$$

$$\Phi_{G,I,J,D} = c\Phi_{G,I,J,n+1,K} + (1-c)\Phi_{G,I,J,n,K}. \qquad (2\text{-}41)$$

If $a = b = c = \tfrac{1}{2}$, the method of solution is called the "diamond-difference method", and if $a = b = c = 1$, it is the "step-function method"[16].

If the diamond-difference equations are combined with equation (2-35), a solution for the fluxes can be found. For the final form of these equations, the reader is referred to the appendix. Through the application of these equations, the complete flux array for a given source can be determined. The order of calculation, called the mesh sweep, is determined primarily by the sequence of cosines, $\bar{\mu}_D$ and $\bar{n}_D$. Detailed information concerning this sequence can be found in the work of Mynatt, et al.[8].

CHAPTER III

THE DOT CODE

DOT (Discrete Ordinates Transport) is a general-purpose Fortran IV program which solves the energy-dependent, Boltzmann transport equation for two-dimensional r-z, x-y, or r-θ geometries. The basic form of the solution is the flux, $\bar{\bar{\phi}}(r_i, z_j, E_g, \Omega_d) \Delta E_g = \phi_{ijgd}$, averaged in the spatial interval surrounding r_i, z_j, integrated over the energy group g, and averaged in the solid segment surrounding Ω_d.

As outlined in the previous chapter on the discrete ordinates method, the gradient or convection term in the Boltzmann equation is approximated by a finite-difference technique. The in scatter integral is approximated by expanding the differential cross-section in a Legendre series which allows the integral to be computed by quadrature. The diamond-difference technique provides the additional relations needed for a solution.

Selection of Code

The general purpose nature of the DOT code was instrumental in its selection as a means of calculating the neutron flux within the small subcritical assembly. Not only can it solve the problem at hand, but once mastered and adapted to the computer system at LSU, it will be an invaluable tool for the Nuclear Science Center in treating a wide variety of problems.

DOT will calculate either scaler or angular flux, or if one desires, the adjoint flux so important in perturbation theory. Adjoint fluxes are proportional to the gain or loss in reactivity of a reactor

32

due to the insertion or removal of one neutron per second at a parti-cular point in the system[17].

DOT will solve inhomogeneous problems which may have either a volume distributed source or a specified angular flux at the right or top boundaries. Fissions may also be included for a subcritical system. Problems consisting of homogeneous systems (eigenvalued prob-lems), may be solved with DOT. The user has a choice of the following alternatives to be calculated:

1. The static multiplication factor, "k" (ratio of sources to losses in the time independent Boltzmann equation);

2. Determination of α in time absorption, α/v, where v is the neutron velocity and α is a number (related to the reciprocal of the reactor period) such that

$$\phi(\vec{r},\vec{\Omega},t) = \phi(\vec{r},\vec{\Omega})e^{\alpha t} \quad (2)$$

3. Fuel concentration necessary to obtain a specified k.

4. Zone thickness for a specified k.

A variety of boundary conditions may be imposed, and activities induced within the system are readily available[18]. The usefulness of such a computer code for nuclear engineering studies is obvious.

The advantage of transport theory over diffusion theory in certain situations has already been mentioned. In particular, calcula-tions of the neutron flux within the fuel cells themselves are more valid when transport theory is applied. Since the flux is rapidly varying due to the absorption of neutrons by the surrounding fuel, the DOT code is better suited than a diffusion code to handle the problem.

The DOT computer code package was obtained from the Radiation Shielding Information Center (RSIC) at Oak Ridge National Laboratory.

The code package contains both a referenced document and a reel of magnetic tape on which is written in separate files: (1) the source card decks; and (2) binary coded decimal (BCD) input and output listing from a sample problem. The version obtained, CCC-89C/DOTII, is operable on the LSU IBM 360/65 Operating System using OS-360 Fortran H Compiler.

Features Within the Code

DOT was first made available in 1966. Since that time, the code has undergone various improvements in technique. The DOT-II version, made available in 1969, possesses interesting features which, among other things, accelerate convergence and corrects for any negative fluxes that may be calculated. The general-purpose nature of the code results from its many built-in options, allowing the user to select those which pertain to his particular problem.

The following sections will outline some of the various techniques within DOT, and illustrate their importance in obtaining valid results. The options built into the code will be mentioned, and the actual flow of calculations within the program will be presented by a flow chart and an explanation of the purpose of some of the key subroutines.

Negative Flux Fix-up

Recall that under certain circumstances it is possible for negative fluxes to be calculated in the discrete ordinates method. In particular, if the flux is decreasing rapidly such that the centered flux is less than half the magnitude of the previous end point flux,

the extrapolated end point flux will be negative, a phenomenon called "diamond-difference breakdown". If this situation exists throughout the system, then the space-angle mesh is inadequate and must be refined. In spite of this correction it is still possible (especially for penetration problems) to generate negative fluxes which have no physical significance.

The simplest method for "negative flux fix-up" is to use the step-function option (where $a = b = c = 1$ in equations $(2-37)$ to $(2-41)$), which always give positive fluxes when the incoming fluxes and the source are positive. DOT employs difference equations based on the "diamond-difference" method as standard procedure, and if a negative end point flux is generated for any point, all fluxes for that cell are immediately recalculated using the "step" equations. This technique is valid for problems where the space-angle mesh is, for the most part, adequate or more than adequate for accurate calculations using "diamond difference"[8].

In addition to the "mixed-mode" method described above, DOT also provides options for using the linear diamond-difference method only or the step-function method only. A comparison of the calculational results using the mixed mode and the linear diamond-difference mode for different sized mesh intervals is illustrated by Figure 7[8]. The problem is one of neutron transport in a water slab exposed to an isotropic fission surface source. Notice that the mixed-mode calculation is always as good or better than the pure linear mode.

Acceleration of Convergence

There are three levels of iteration in DOT: inner iteration for within group scattering, fission source iteration, and iteration
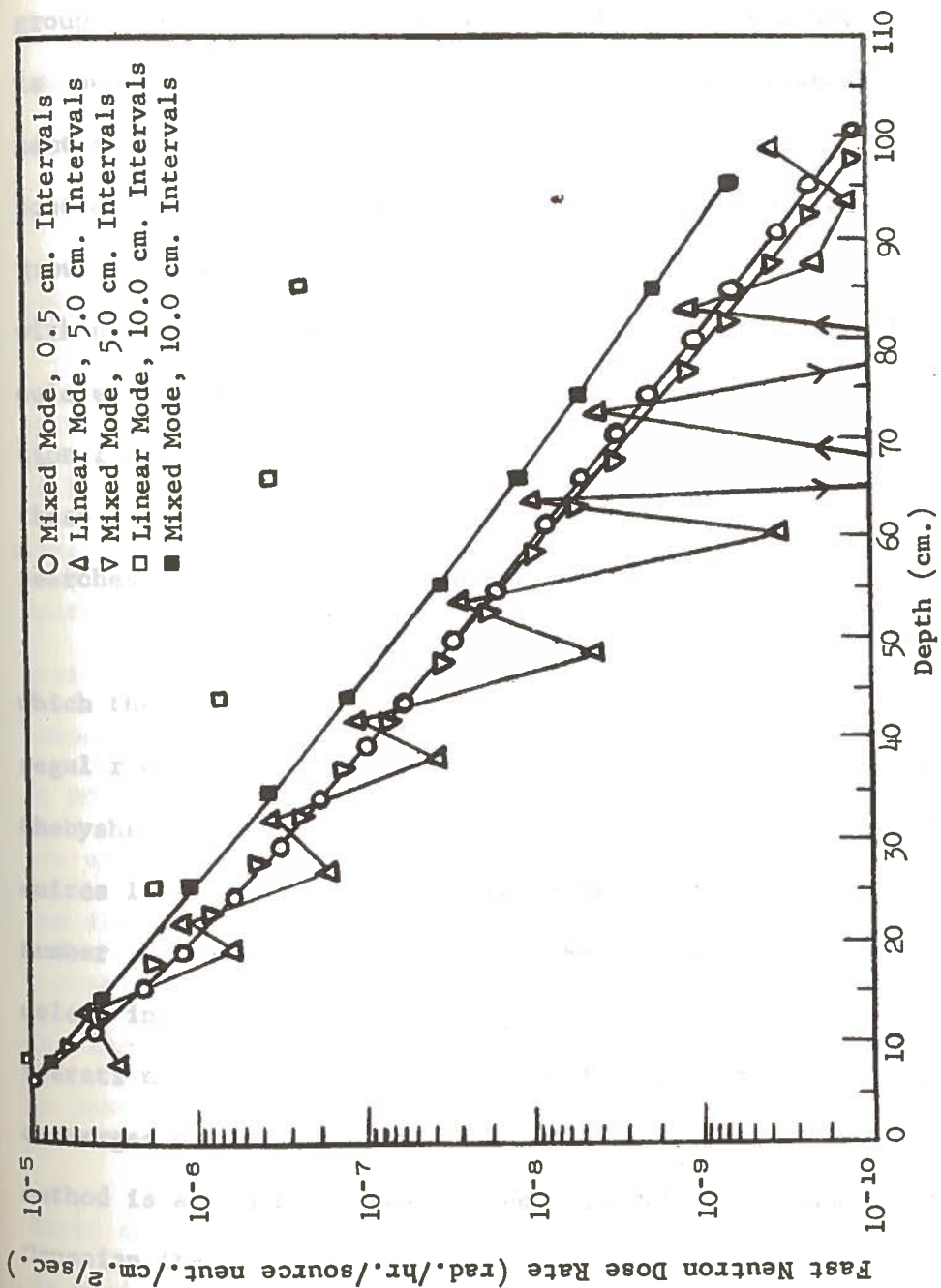
FIGURE 7. The Effects of Mesh Spacing and Difference Model on the Calculated Fast Neutron Dose Distribution in a Water Slab

36

for eigenvalue searches. If one assumes that particles undergoing scattering always degrade in energy, then the flux of the highest energy group should be calculated first, the second highest energy group next, and so on. The downscatter source for any particular group is completely determined, and may therefore be treated as a fixed component in the source for the next lowest energy group. The within-group scattering for any group involves fluxes yet to be determined for that group, and inner iterations are necessary. If fissions are present within the system, the fission source is determined by the flux calculated by inner iterations, and this source then constitutes an additional source which requires a repeat of the inner iterations until these outer fission iterations converge. The iteration for eigenvalue searches are of no concern here and will not be described.

The DOT code incorporates a choice of four techniques by which the scalar flux solution may be converged on inner iterations: regular or Gaussian, successive overrelaxation, point-scaled, and Chebyshev[6]. The Gaussian iteration is the simplest method and requires less core storage than the others, but also requires the greatest number of iterations to converge. Successive overrelaxation is an accelerating technique which is applied after every fourth Gaussian iteration. Except for deep penetration problems, this method usually converges more quickly than the Gaussian technique. The Point-scaled method is a technique which is applied after a predetermined number of Gaussian iterations have been completed. This method is particularly useful for deep penetration problems. Chebyshev acceleration is applied every iteration after the third Gaussian iteration[19].

The user of the DOT code must choose the acceleration technique that fits his problem. In general, the Chebyshev acceleration technique should not be used. For difficult problems, and in problems where data storage is not a limiting factor, the point-scaled method should be used. Where data storage is limited, successive overrelaxation is best. The Gaussian technique can be used for simple problems or those plagued by extreme data storage limitations[18].

Additional Improvements

The approximations made in the development of discrete ordinates transport do not limit the accuracy of the method, since, at least in principle, the number of energy groups, solid angle segments and space intervals, and the order of expansion of the differential scattering cross sections may be increased as necessary to obtain the desired solution. In practice, the only limiting factor is the finite computer speed and memory size. In order to extend the capabilities of DOT, a combination of efficient programming and analytical techniques are used. The programming techniques involve methods for efficient and flexible allocation of the main computer memory, handling of large blocks of data on external storage devices, and the concentration of the innermost loops into a single, small subroutine which is programmed in assembler language.

One of the analytical techniques used in DOT is the analytic first collision source. This technique reduces the "ray effect", which is noticeable in a problem with a source that is small compared to the total geometry. Another technique that can be used in DOT is the introduction of a biased quadrature set. In some problems, such a set

will give significantly better results than a symmetrical quadrature set[8]. DOT can also be used to determine the flux in an external void outside of a shield.

The DOT Program Itself

The nature of the physical problems that DOT solves and the general techniques used have already been discussed. Theoretically, the solution of the linear Boltzmann transport equation will approach the exact solution with increasing orders of approximation as the space, angle, and energy mesh approaches differential size.

The DOT code utilizes variable dimensioning to allow dynamic core data storage allocation at execution time, thus eliminating the necessity for recompilation for different size problems. Because of this variable dimensioning technique, no size restriction is imposed on any given data array, only on the length of the sum of all arrays[19].

The DOT-II code is written in standard FORTRAN IV, with the exception of one of the subroutines, GRIND, which is also available in COMPASS assembler language[19]. GRIND contains most of the computations, and the assembly version allows problems to run two or more times faster than the all-FORTRAN version[19,20].

The DOT input is divided into nine data sets[20]:

1. Overall problem storage allocation, tape and disk assignments, and boundary source input tape parameters

2. Problem title and parameters specifying code options

3. Cross section data

4. Initial flux guess data

5. Fixed distributed source data

6. Fixed boundary source data

7. Angular quadrature (direction cosine: μ, η) data

8. Angular quadrature (weight: w) data

9. Remainder of data.

Data set No. 1 is entered on the "units assign card", the first data card. Data set No. 2 consists of the title card and 43 fixed parameters on the next nine cards. The remainder of the data sets are read in the form of data arrays, but not all of these data arrays are necessary for any given problem.

The use of an adequate mesh spacing in a DOT calculation is necessary to obtain an accurate solution utilizing as little core as possible. Too large a spacing would result in the generation of the negative fluxes discussed earlier, while two small a spacing would needlessly waste core and computer time. Westinghouse Electric Corporation has developed empirical relationships for approximating maximum mesh interval spacing[19].

The importance of obtaining flux convergence in the inner iterations cannot be overstated. In problems with scattering to a higher energy (upscatter) or fission sources, the outer iterations proceed on the basis of inner iteration convergence. A good initial estimate for the flux will accelerate the convergence of these inner iterations[19].

The overall flow diagram of DOT is shown in Figure 8, and Table II briefly describes the function of the principal subroutines in DOT[19].
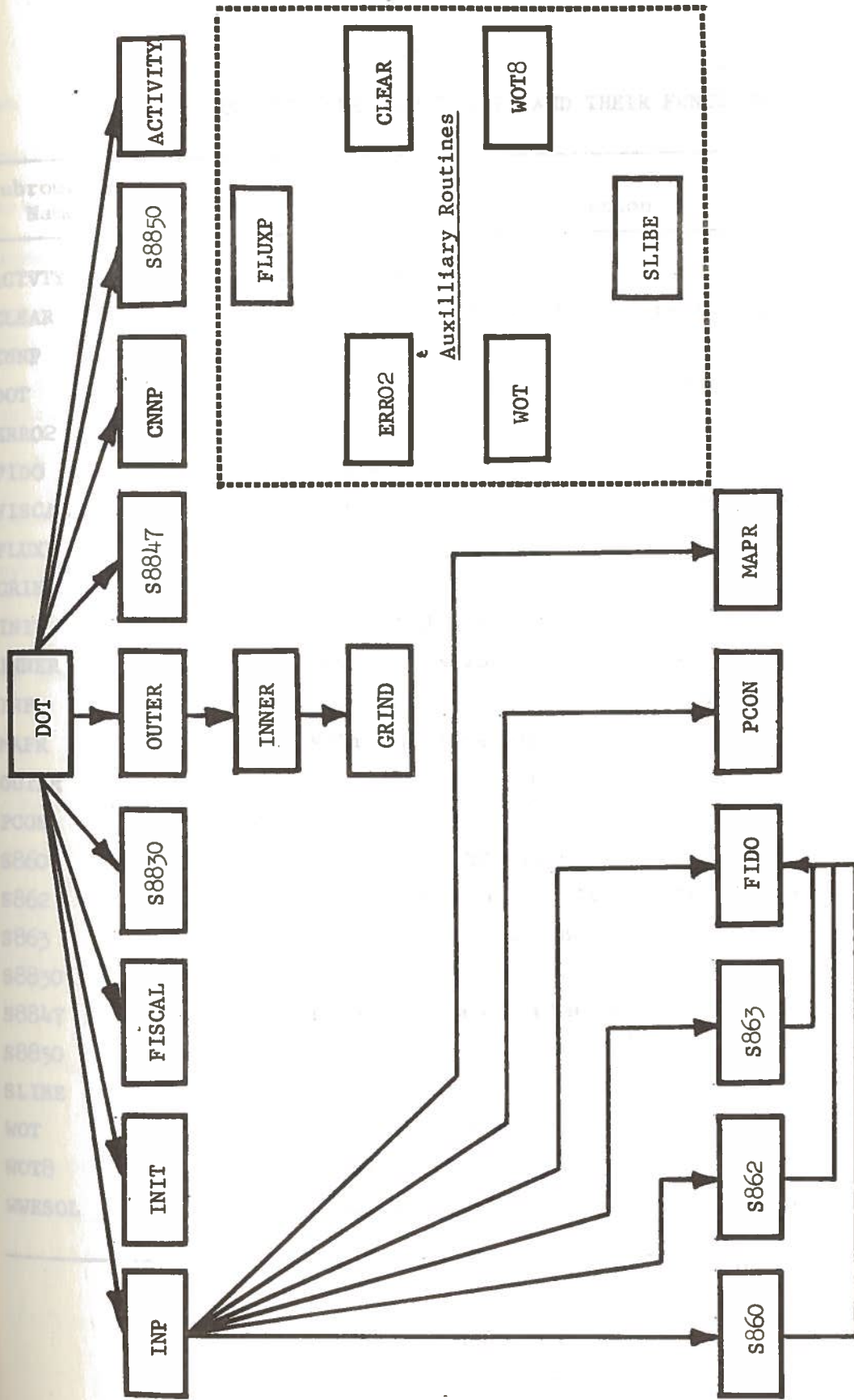
FIGURE 8. Flow Chart for the Two-Dimensional, Discrete Ordinate Transport Program, DOT

41

TABLE II

LIST OF DOT CODE SUBROUTINES AND THEIR FUNCTION

Subroutine Name	Function
ACTVTY	Activity Calculation
CLEAR	Clears Discrete Areas of Core Storage
CNNP	Covergence Tests and Upscatter Scaling
DOT	Overall Control of Program Information Flow
ERRO2	Writes Error Messages
FIDO	Generalized Input Read Routine
FISCAL	Fission Sum Calculation and Normalization
FLUXP	Angular Flux Print
GRIND	Inner Iteration Calculation
INIT	Inital Calculations and Setup
INNER	Inner Iteration Control
INP	Variable Dimension and Input Data Read Control
MAPR	Prints Picture Plot
OUTER	Outer Iteration Control
PCON	Calculates P_L Coefficients
S860	Reads Cross Sections
S862	Reads Fluxes and/or Distributed Source
S863	Reads Top or Right Boundary Source
S8830	Monitor Line Printout
S8847	Group Totals Calculation
S8850	Final Print
SLIBE	Tape Cross Section Read Routine
WOT	General Print Routine
WOT8	General Print Routine
WWESOL	Iteration Control During Point Scaling

The computer printout of a DOT calculation is contained on an on-line printer and, if desired, on two binary tapes. The first part of the printed output is a listing of the input data. All parameters and data arrays are printed along with two-dimensional zone and material maps. The value of LAST, the amount of variable dimension data storage locations used in the problem, is also printed.

The remainder of the printed output consists of quantities calculated by DOT. Of these, the one of particular interest in this problem is the scalar fluxes. These are printed for every spatial mesh point by energy groups. Besides having the flux data available in the printed output, both the scalar and angular fluxes may be read out on tape. This is especially useful if one plans to use this data as input to another problem or as an initial flux guess for the same problem.

CHAPTER IV

SUBCRITICAL ASSEMBLY

Basic Theory

A subcritical assembly is an arrangement of nuclear fuel and moderator that will not sustain a fission chain reaction. While neutrons from an external source are multiplied by the fission process, the neutron population decreases after the source is removed. In an assembly consisting of light water and natural uranium, the neutron-related characteristics of both the moderator and the fuel prevent the possibility of criticality being reached[21]. A small assembly of this type is very far subcritical due to large neutron leakage.

For a chain reaction to be maintained, the ratio of the number of neutrons of any one generation to the number in the preceding generation must be at least unity. For an infinitely-large system, the requirement is that $k_\infty = 1$, where k_∞ is the infinite multiplication factor. For finite-sized reactors, there is the probability that neutrons may escape, so that $k = k_\infty P$ defines an effective multiplication factor, k, and P is the probability that a neutron remains in the system during a cycle[3].

The measurement of the neutron flux distribution within the assembly allows one to determine various reactor parameters such as the buckling, Fermi age, diffusion length, and migration area. Once these quantities are known, the multiplication factors, k and k_∞ can be obtained.

The buckling, B^2, is a measure of the spatial rate of change of the curvature of the neutron flux at a given point per unit flux. In general, the buckling is defined by

$$B^2 \equiv \left|\frac{\nabla^2 \phi(r)}{\phi(r)}\right|, \text{ at } r \tag{4-1}$$

where ∇^2 is the Laplace operator[22].

There are two different kinds of buckling -- the material buckling, B_m^2, which is a specific property of the materials of the multiplying medium; and the geometric buckling, B_g^2, which involves the size and shape of the reactor. For a critical or near critical system $B_g^2 = B_m^2$, while for a subcritical one, B_g^2 is greater than B_m^{2}[22].

If the subcritical assembly is relatively large, the thermal neutron flux distribution (away from boundaries and extraneous source) can be represented quite closely by the wave equation (3):

$$\nabla^2 \phi(r,z) + B_m^2 \phi(r,z) = 0. \tag{4-2}$$

For cylindrical geometry, the boundary conditions imposed when solving this equation are that the flux is finite throughout the core and vanishes at the extrapolated radius, R. The solution is

$$\phi(r,z) = \phi_0 J_0\left(\frac{2.405r}{R}\right)e^{-\gamma z}, \tag{4-3}$$

where J_0 is the zero-order Bessel function and γ is a constant. The material buckling is related by[3]

$$B_m^2 = \left(\frac{2.405}{R}\right)^2 - \gamma^2. \tag{4-4}$$

If the neutron flux measured along the vertical central line of the assembly is plotted against z on semilog paper, the slope of the

straight line over the region away from the source and the boundary is $-\gamma$ as seen from equation (4-3). Substitution of this value into equation (4-4) allows one to determine the material buckling B_m^2[22].

Other fundamental properties that can be found once the flux distributions are known, are the migration area, M^2, diffusion length, L^2, and Fermi age, τ[23]. These may be experimentally determined independently, or one can use the relation, $M^2 = L^2 + \tau$.

The migration area is the mean square distance from the point of birth as a fast neutron to death in thermal capture[2]. Fermi age is a measure of the distance that a neutron travels before it is thermalized, and diffusion length is a measure of the distance it travels as a thermal neutron[17].

The diffusion length for a subcritical system using internally and externally light water moderated annular natural uranium fuel slugs has been calculated as 1.2 cm[24]. The Fermi age for the system has been found to be 32.5 cm^2[24], thus yielding a migration area of 33.840 cm^2.

If the reactor is assumed to be large and near criticality, then[3]

$$k_\infty = 1 + M^2 B_m \tag{4-5}$$

and

$$k = k_\infty P = \frac{k_\infty e^{-B_g^2 \tau}}{1 + L^2 B_g^2} \cong \frac{k_\infty}{1 + M^2 B g^2} \tag{4-6}$$

where

$$B_g^2 = \left(\frac{2.405}{R'}\right)^2 + \left(\frac{\pi}{H'}\right)^2 \tag{4-7}$$

In equation (4-7), R' and H' are the extrapolated values of the radius

and the height. These extrapolated dimensions measure the size of the
system as it appears to thermal neutrons.

The value of k calculated from equation (4-6) can be used to
determine a subcritical multiplication constant, m. This "m" is de-
fined as the ratio between thermal neutron flux due to both the pri-
mary source and fission, and that due to the primary source alone[22].
The multiplication is

$$m = \frac{1}{1-k}.$$

Assembly Design

The LSU Nuclear Science Center already possesses a large sub-
critical assembly nicknamed the "Tiger Pile". In order to provide a
system with different characteristics, a smaller assembly with fuel
elements that have both internal and external moderation was constructed.
The new assembly would serve as a teaching aid for reactor physics and
radiation shielding studies. Its neutron multiplication properties
could provide a higher flux for short half-life activation analysis
studies than could normally be obtained in pure moderators.

The foremost considerations in the design and construction of
this subcritical assembly, nicknamed the "Mini Pile", were low cost and
utilization of existing materials. The natural uranium fuel slugs used
were left over from the construction of the Tiger Pile. The tank it-
self is constructed from a 55-gallon drum mounted on a caster-equipped
base. All other materials were purchased from local sources for less
than thirty dollars.

The fuel elements used are cylindrical natural uranium slugs on loan from the AEC. These slugs are clad in aluminum jackets .040 inches thick for protection and ease of handling. The cylinders average 8.2 inches in length, and are 1.20 inches in diameter with a .50-inch central hole extending the length of the slug. Each slug contains approximately 3.9 pounds of uranium.

The upper part of the wall of the 55-gallon drum is cut away so that the shortened drum wall is 23 inches high. The interior of the drum is coated with an epoxy* paint to prevent corrosion and water leakage.

The rods are held in a vertical position by an epoxy-painted wooden plate on the bottom, and aluminum strips at the top (see Figure 9). No nuts or fasteners of any kind are used; the holes in both the bottom plate and the aluminum strips are drilled so that a close fit is provided. Three other aluminum strips are used to brace the forest of rods against the side of the tank.

The fuel rods consist of two slugs secured end-to-end by a 3-inch strip of .50-inch o.d. Plexiglas† tubing. The Plexiglas tubing is slit lengthwise in order to decrease its diameter slightly so that it fits snugly within the fuel slugs. The same size tubing is inserted in both ends of the fuel rod for mounting in position as in Figure 9. This type of plastic was chosen because its neutronic characteristics are similar to those of water.

---

* "CHEM-O-PON Epoxy Coating", manufactured by Jones-Blair Paint Co., Inc.

† Registered trademark for acrylic sheet manufactured by Rohm and Haas Company.
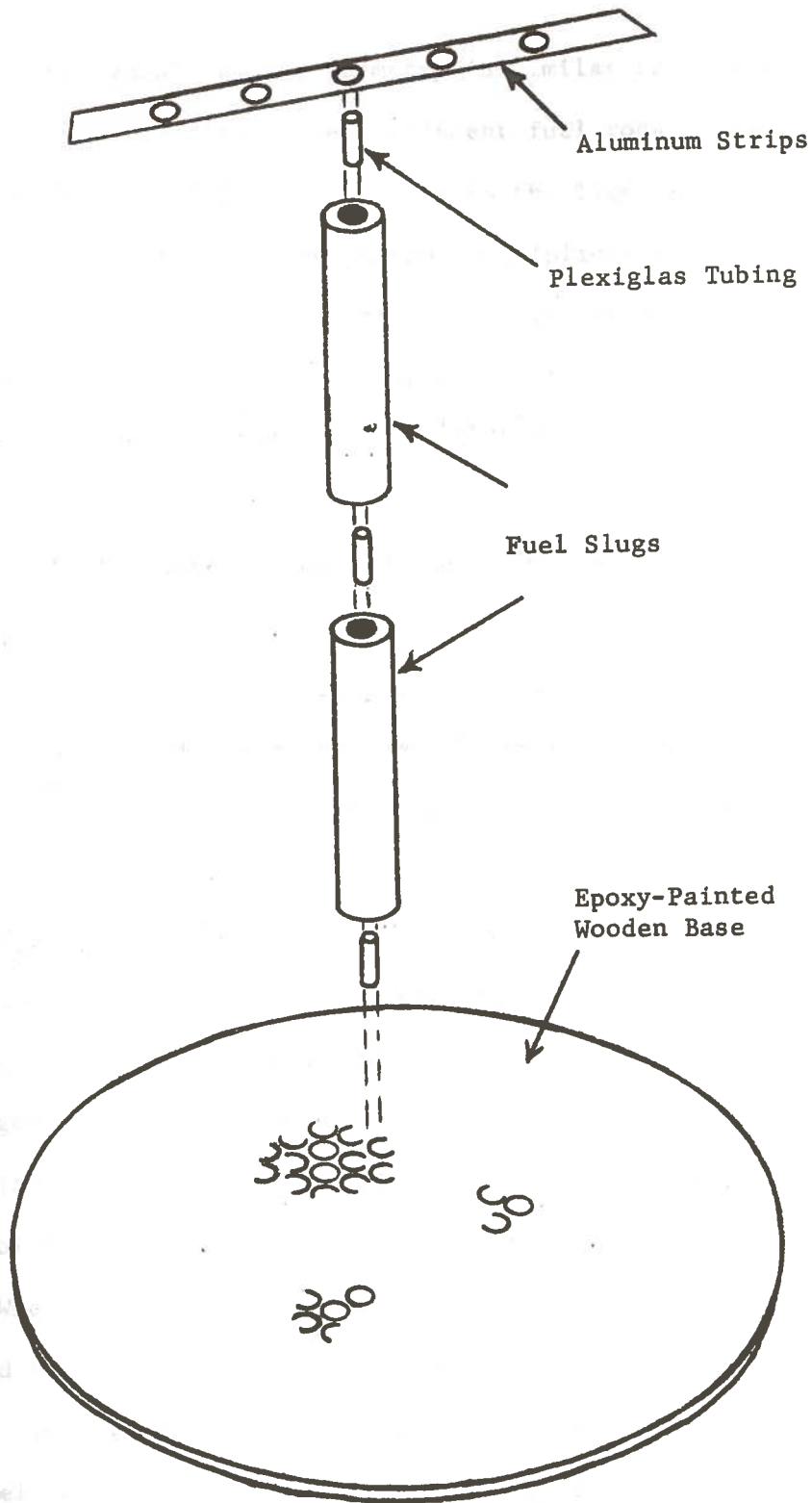
FIGURE 9.   Fuel Rod Assembly

The hexagonal lattice geometry is similar to that of the Tiger Pile, but the spacing between adjacent fuel rods is smaller (Figure 10). The actual lattice spacing in the Tiger Pile is greater than the theoretical spacing for maximum multiplication because of the necessity of allowing for passage of the neutron detector[25]. A tighter lattice to increase neutron multiplication was suggested[26], and previous work support this proposal[24,27].

A useful feature of the Mini Pile not found in the Tiger Pile is the access to the interior of the fuel elements. The plastic tubing inserts have 3/8-inch nominal inner diameter, sufficient to allow passage of the 3/8-inch diameter BF_3 probe. This provides easier and more accurate positioning of the probe, and allows one to study the self-shielding of the uranium fuel. The fuel is moderated both internally and externally with light water.

The source holder, also constructed of Plexiglas, is designed to accommodate both PuBe and Cf-252 external neutron sources (Figure 11). The polyethylene cylinder, which serves as a source stop, is of the proper length so that the source position corresponds to the axial mesh block specified in the input for the DOT code. A tapered hole in the upper end of the cylinder allows for easy positioning of the californium capsule. When a PuBe source is used, it is merely inserted into the holder, and the three flat Plexiglas strips guide it onto the polyethylene stop. The holder itself is attached to the innermost hexagonal ring of fuel rods by the holes in the upper plate of the holder.
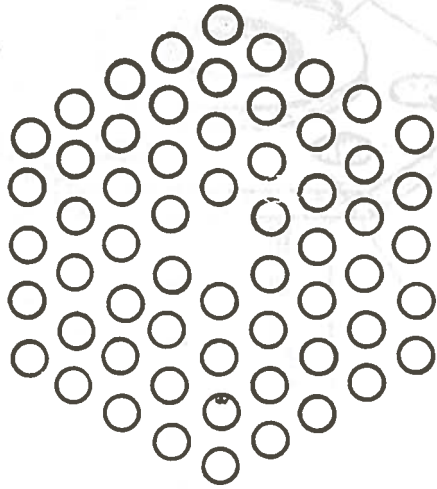
Hexagonal Lattice
60 Fuel Rods
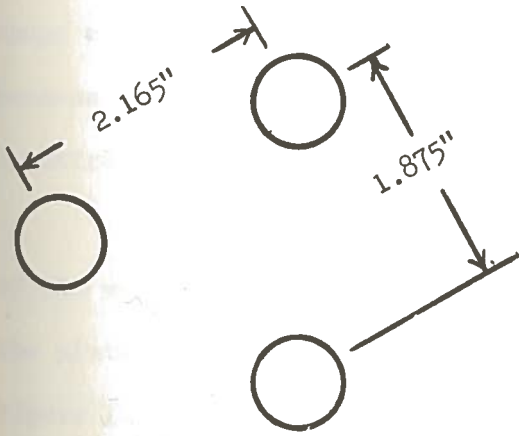
Tiger Pile
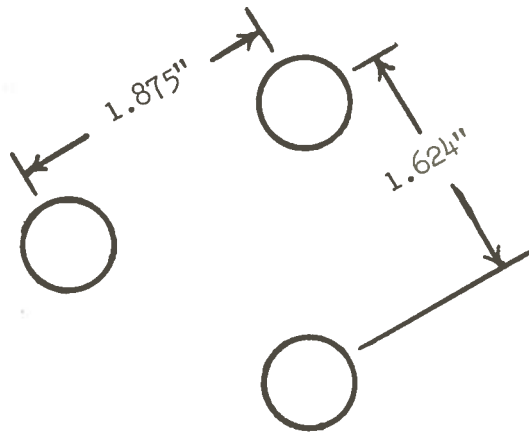
Mini Pile

FIGURE 10. Lattice Geometry and Spacing

For Tiger Pile and Mini Pile

Annular Ring

6.4 cm

Holes for
Fuel Rods

4.8 cm

Hexagonal Plate

Flat Strips

42.9 cm

Tapered Hole

21.3 cm

Polyethylene Source
Stop and Positioner

Hexagonal Plate
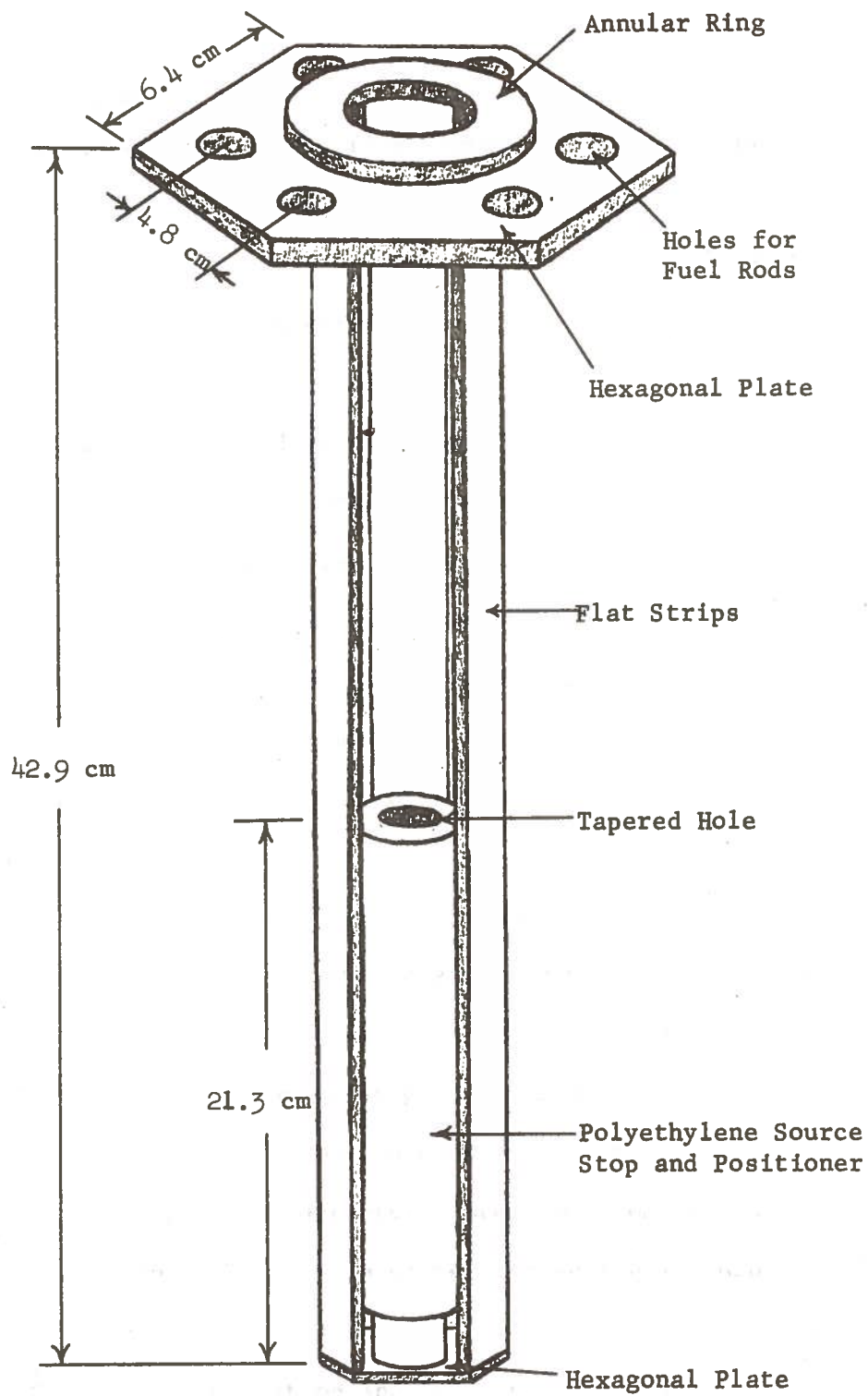
FIGURE 11.   Plexiglas Source Holder

52

Measurement Techniques

The measurement of the flux distribution within the Mini Pile
was accomplished through the use of a Nuclear Chicago Model NC202 BF_3
probe and associated counting equipment. A trolley and track assisted
in accurately positioning the detector.

The boron trifluoride (BF_3) gas-filled detector uses the B^{10}-
$(n,\alpha)Li^7$ reaction for thermal-neutron detection. The alpha particle
and the recoil lithium nucleus produce ionization within the gas, and
the resulting voltage pulse is amplified and fed into a scaler. The
block diagram for the circuit is shown in Figure 12. The cross-section
of the reaction (Figure 13), the simple energy dependence over a wide
range of energy values, and the ability to count in high gamma fluxes
because of the difference in specific ionization, make the BF_3 detector
an attractive neutron counter.

In order to insure a count rate that is relatively independent
of the voltage applied to the tube, one must operate the detector on
the plateau region of the curve of count rate vs voltage as shown in
Figure 14. The discriminator setting on the scaler must be adjusted
so that most of the smaller gamma-induced pulses are rejected.

Calibration of the detector system is accomplished through
foil activation methods[28]. A point neutron source is suspended in
the moderator, and a comparison is made between the flux distribution
obtained through foil activation and the count rate of the detector
system. This provides a value for the sensitivity of the detector sys-
tem (the number of flux units corresponding to one count per second by
the detector).
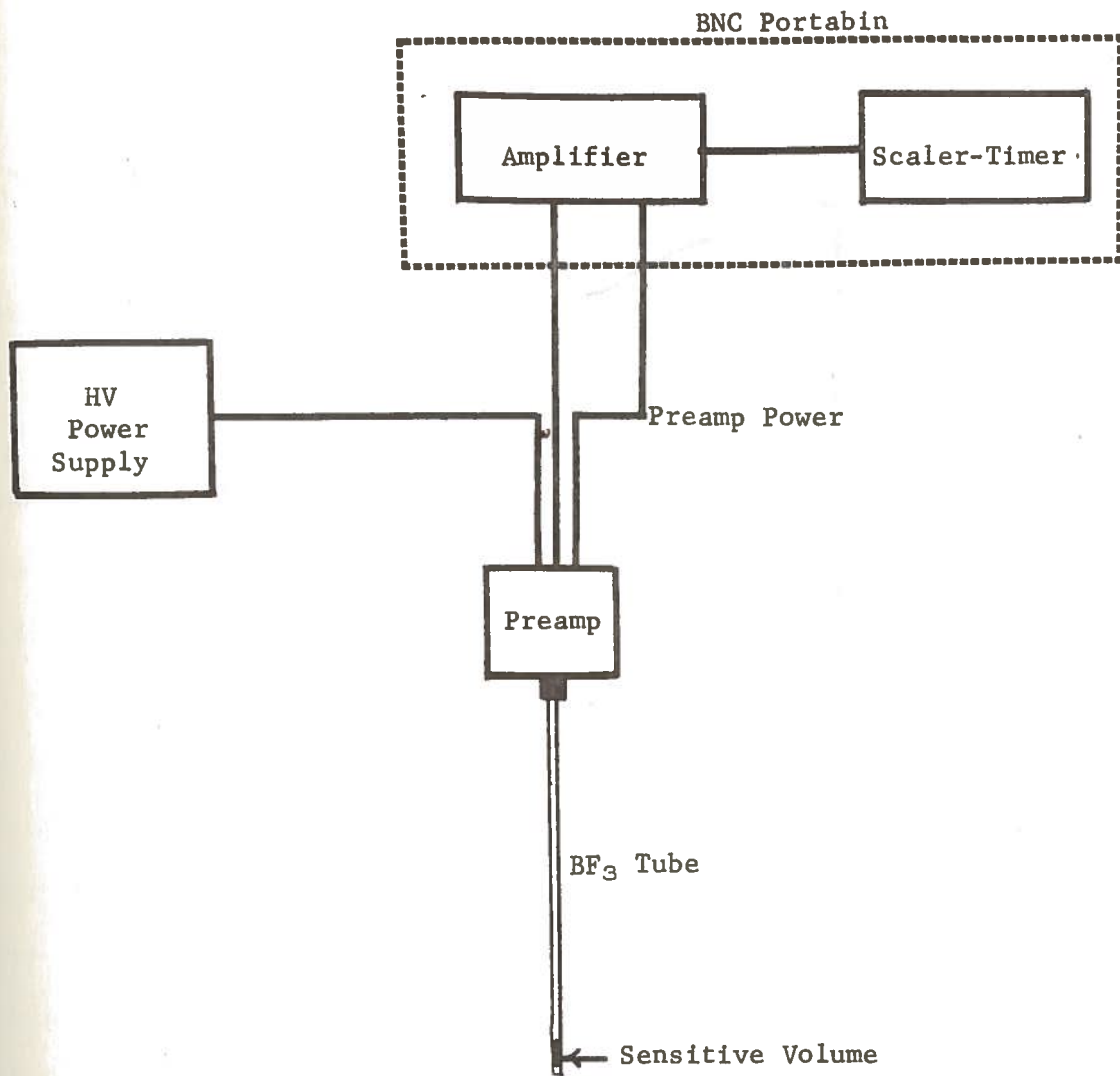
DCHV Power Supply - Canberra Model 6516 A

Amplifier - Canberra Model 816

Scaler-Timer - Canberra Model 895

Instrument Case and Power Supply - Berkeley Nucleonics Corp. Portabin
                                   Model AP-1

Preamp - Stabilized 3-transistor, high gain, low output impedance;
         made by J. J. Philips, LSU Nuclear Science Center

BF_3 Tube - Nuclear Chicago NC202

FIGURE 12. Block Diagram of BF_3 Detector System
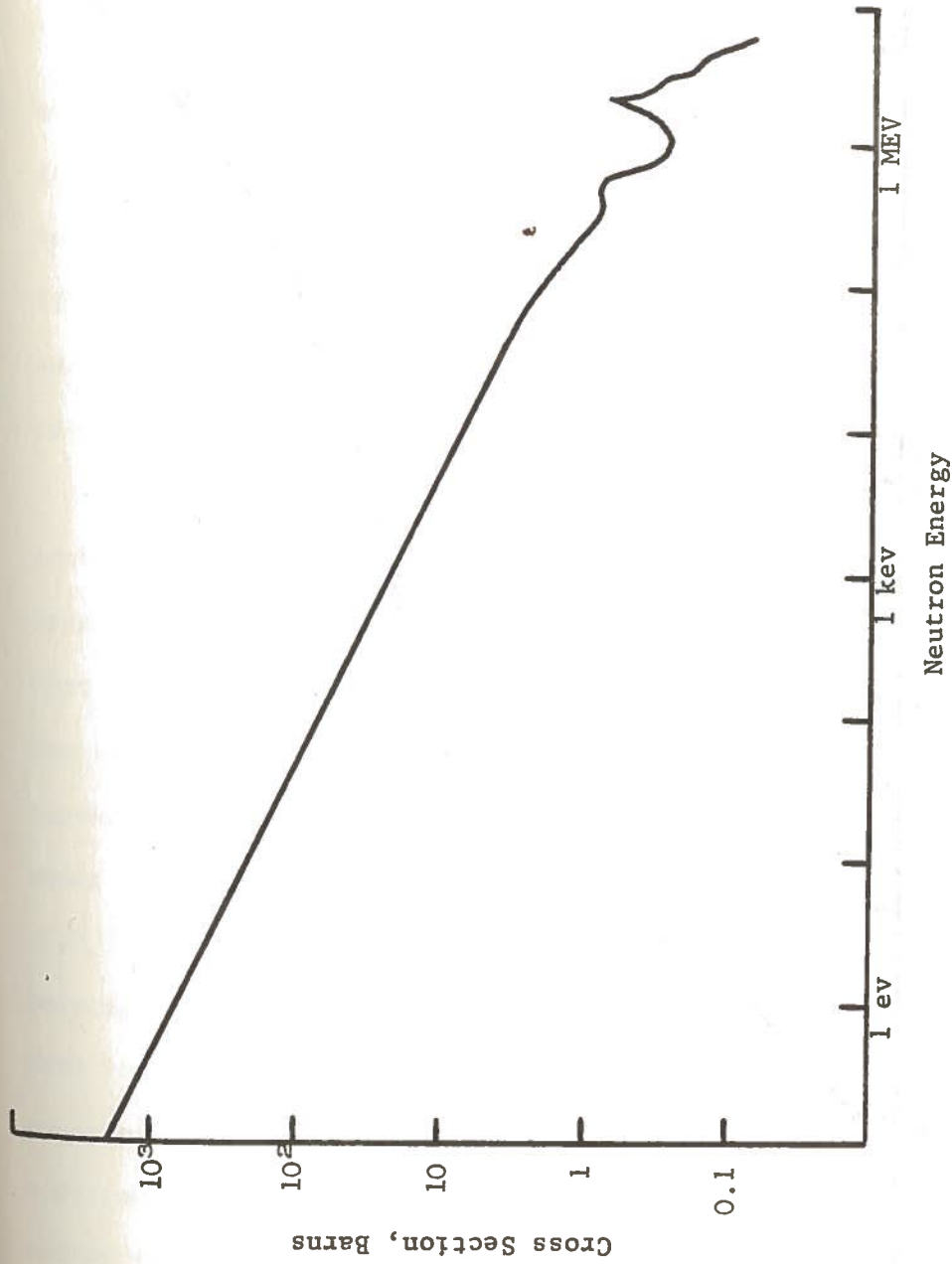
FIGURE 13. Cross Section versus Neutron Energy for the $B^{10}(n,\alpha)Li^7$ Reaction
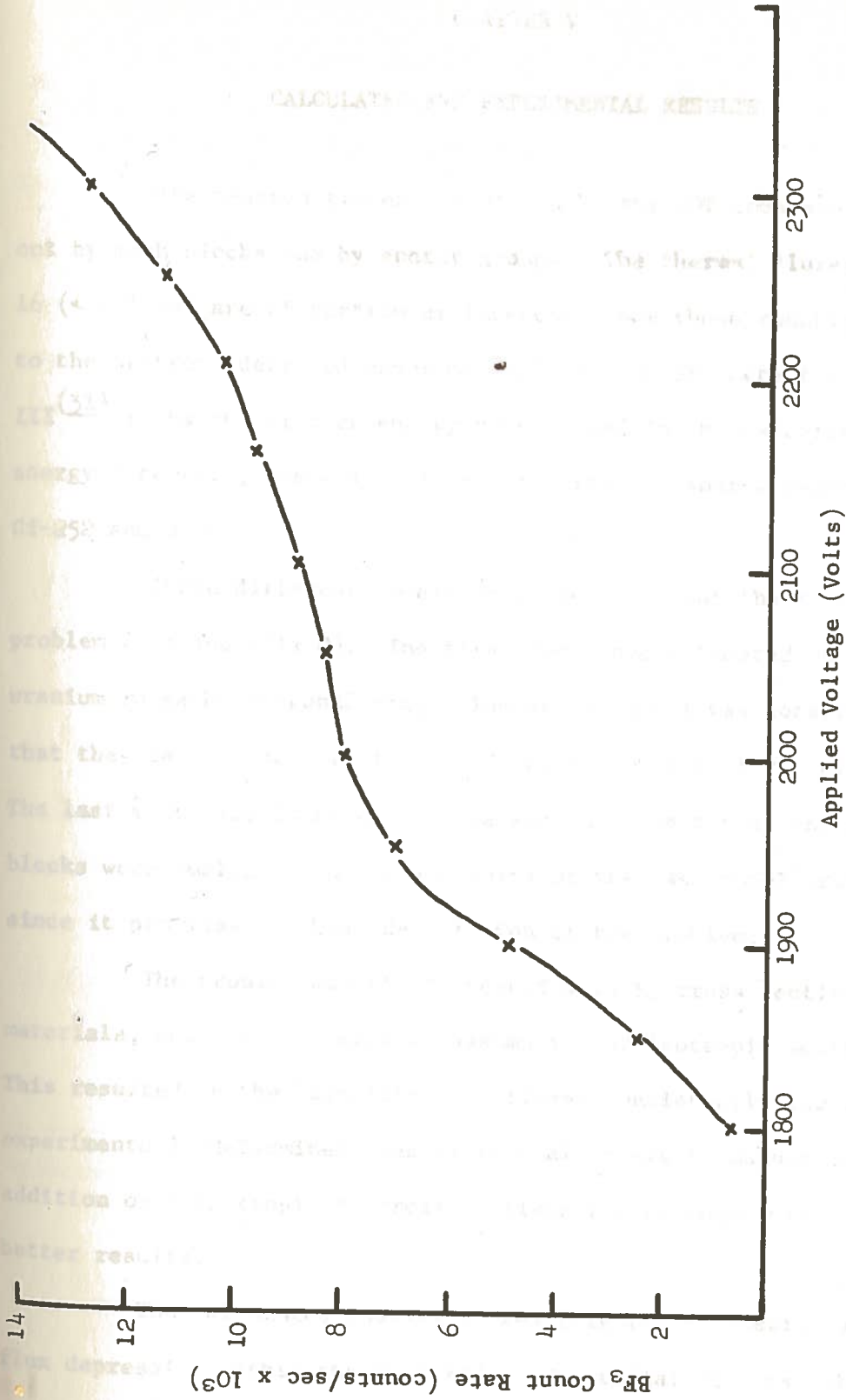
FIGURE 14. Plot of Count Rate versus Applied Voltage for NC202 BF$_3$ Tube

CHAPTER V

CALCULATED AND EXPERIMENTAL RESULTS

The neutron fluxes calculated by the DOT code are printed out by mesh blocks and by energy groups. The thermal fluxes of group 16 (< 0.1 ev) are of particular interest since these roughly correspond to the neutrons detected experimentally by the BF_3 detector. Table III[31] lists the sixteen energy groups used in the calculations by energy intervals, and also compares the fission source neutron of Cf-252 and U-235.

Three different models were used to treat the Mini Pile problem (see Appendix C). The first model overestimated the amount of uranium in each hexagonal ring. The second model was constructed such that the uranium/water ratio was identical to that of the Mini Pile. The last model was identical to the second, except that the axial mesh blocks were smaller. Only the results of the last model are presented, since it provides the best description of the problem.

The problem was first treated with P_O cross sections for all materials, which is actually an assumption of isotropic scattering. This resulted in the calculation of fluxes consistently lower than the experimentally-determined ones by several orders of magnitude. The addition of anisotropic P_1 cross sections for hydrogen yielded much better results.

The calculated thermal fluxes (Figure 15) clearly show the flux depression within the fuel rods. The radial traverse above the rod region illustrates a deflection of the flux near the fuel rods.

TABLE III

GROUP STRUCTURE AND FISSION NEUTRON SOURCE SPECTRA OF Cf-252 AND U-235

| Group | Energy Interval | Energy Distribution | |
		Cf-252	U-235*
1	3-∞ MeV	0.2308	0.204
2	1.4-3 MeV	0.3570	0.344
3	0.9-1.4 MeV	0.1789	0.168
4	0.4-0.9 MeV	0.1954	0.180
5	0.1-0.4 MeV	0.0328	0.090
6	17-100 keV	0.0051	0.014
7	3-17 keV		
8	0.55-3 keV		
9	100-550 eV		
10	30-100 eV		
11	10-30 eV		
12	3-10 eV		
13	1-3 eV		
14	0.4-1 eV		
15	0.1-0.4 eV		
16	0-0.1 eV		

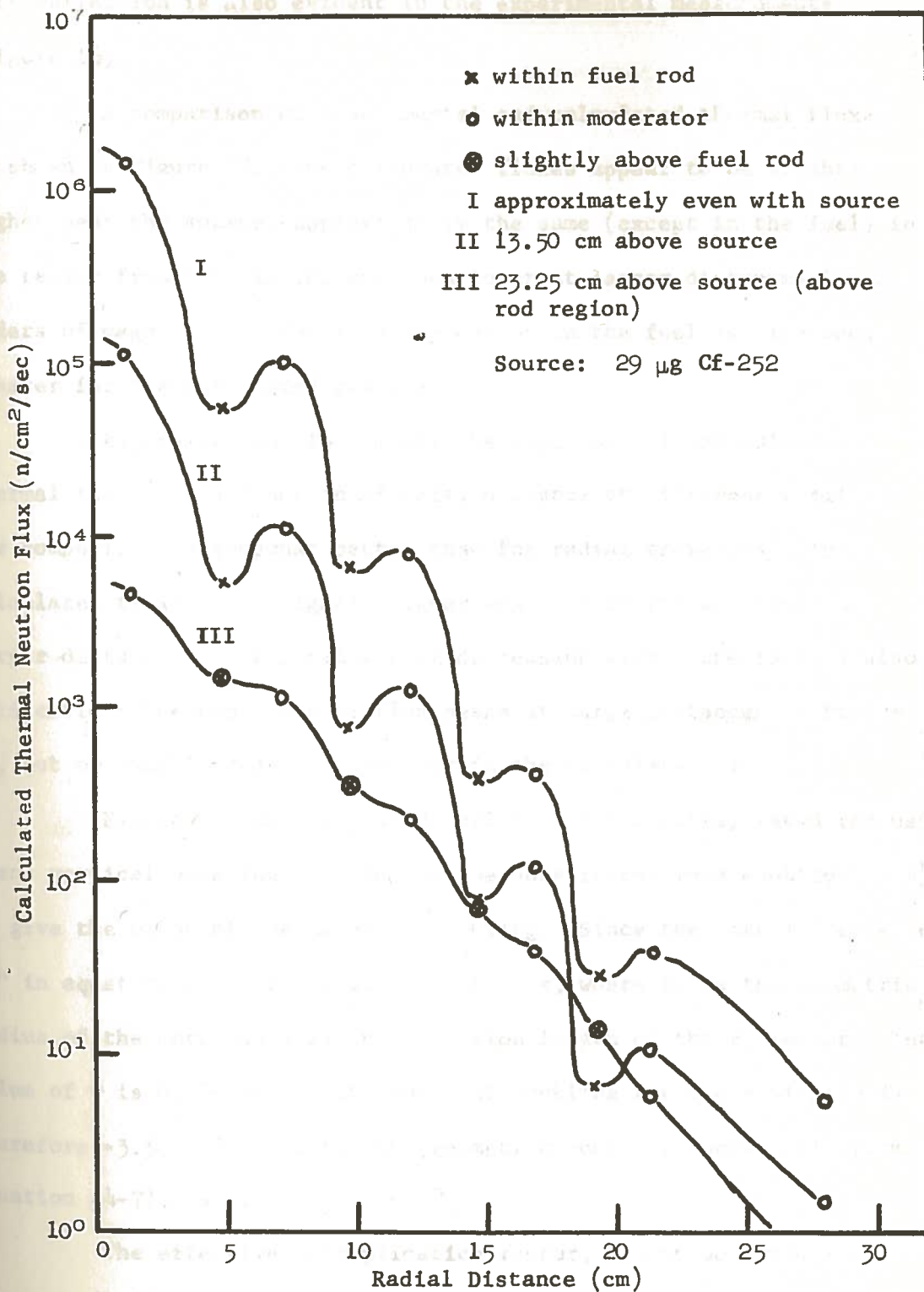*Spectrum given for U-235 is appropriate for thermal neutron fission.

58

FIGURE 15. Calculated Thermal (< 0.1 ev) Neutron Flux _versus_ Radial Distance for Various Heights.

59

This deflection is also evident in the experimental measurements (Figure 16).

A comparison of experimental and calculated thermal fluxes is shown in Figure 17. The calculated fluxes appear to be slightly higher near the source, approximately the same (except in the fuel) in the region from 5 to 10 cm, and much lower at larger distances (by 2-3 orders of magnitude). The flux depression in the fuel is also much greater for the calculated results.

Figures 18 and 19 compare the experimental and calculated thermal fluxes as a function of axial distance at different radii. The comparison is somewhat better than for radial traverses. Again, calculated fluxes are slightly higher near the source and lower at larger distances. The greater flux depression within the fuel is also noticeable. The experimental flux peaks at large distances in Figure 19, but no such increase is apparent in the calculated flux.

Figures 20 and 21 provide values for the extrapolated radius R and vertical buckling γ, which may be substituted into equation (4-4) to give the value of the material buckling. Since the core is reflected, "R" in equation (4-4) is replaced by $R_O + s$, where R_O is the geometric radius of the core and s is the diffusion length of the reflector. The value of γ is 0.120 cm^{-1}. The material buckling for the Mini Pile is therefore -3.30×10^{-3} cm^{-2}. The geometric buckling, obtainable from equation (4-7), is 1.62×10^{-2} cm^{-2}.

The effective multiplication factor, k, can be found from equation (4-6). A value of k_∞ obtained for similar lattices is assumed[24,27], and, using a value of 33.84 cm^2 for the migration area, the value of k is
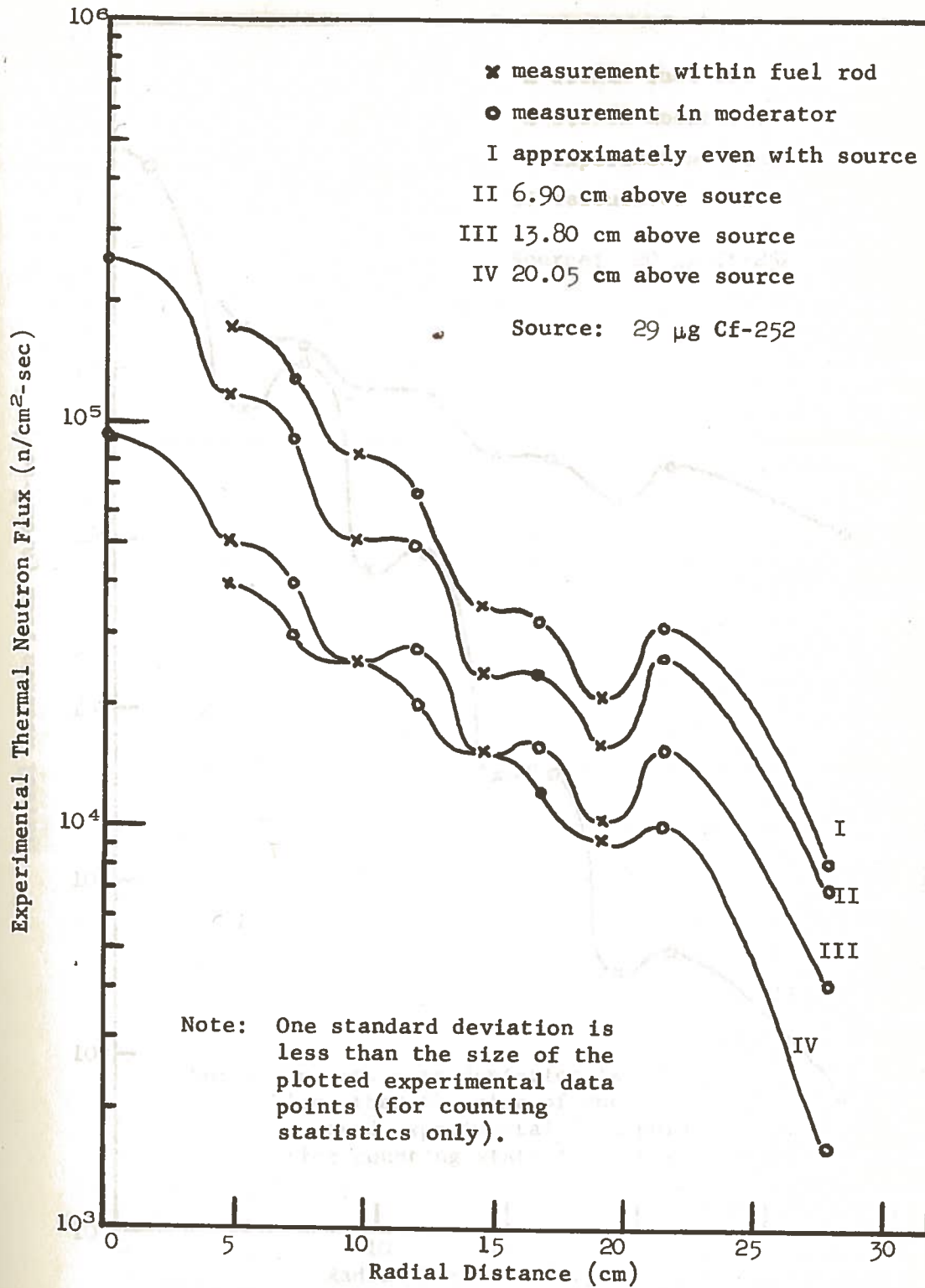
FIGURE 16. Experimental Thermal ($< \sim 0.1$ ev) Neutron Flux
versus Radial Distance for Various Heights.
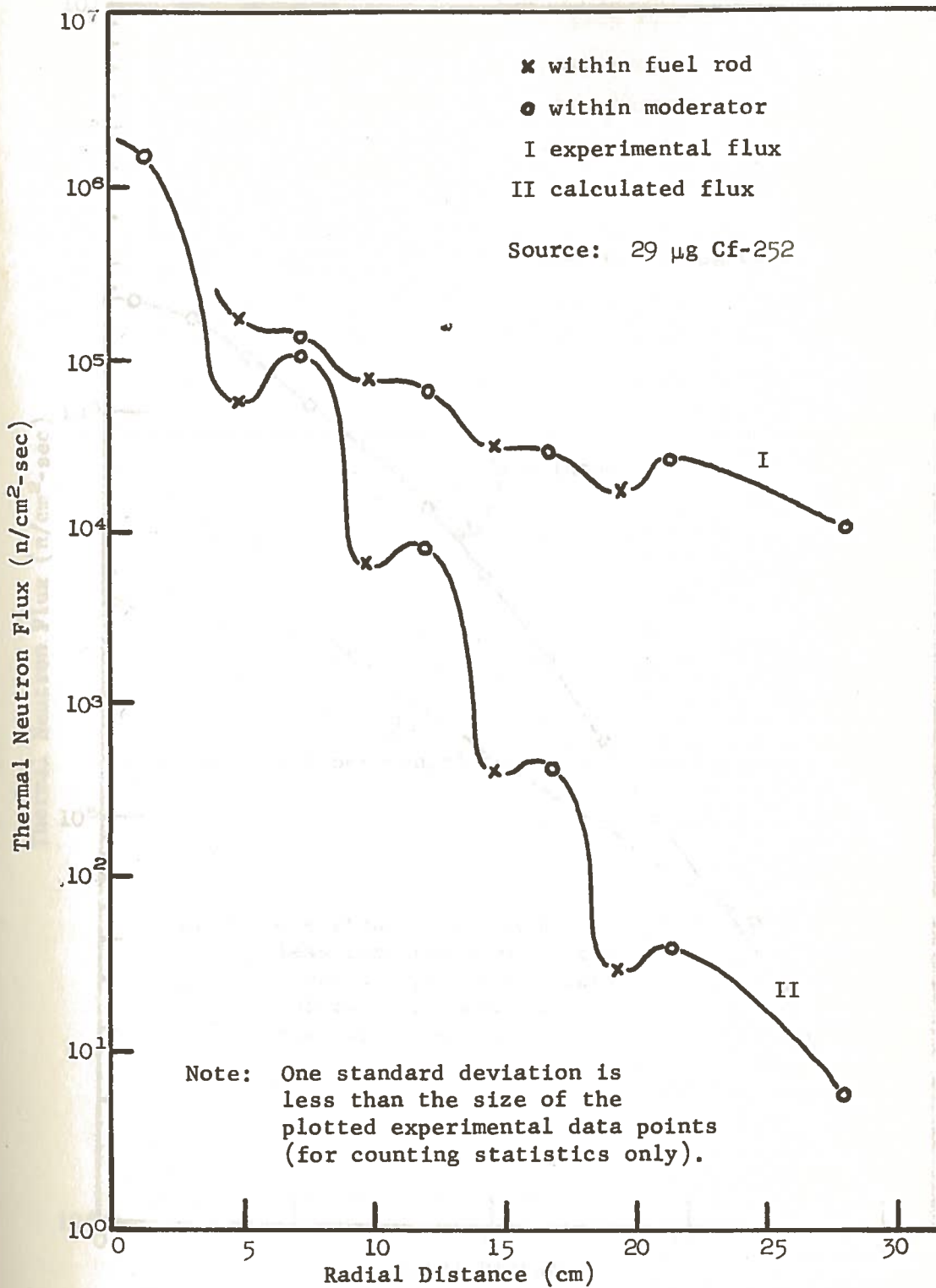
FIGURE 17.   Comparison of Experimental and Calculated Thermal
            (< 0.1 ev) Neutron Fluxes as a Function of Radial
            Distance Even with Source.
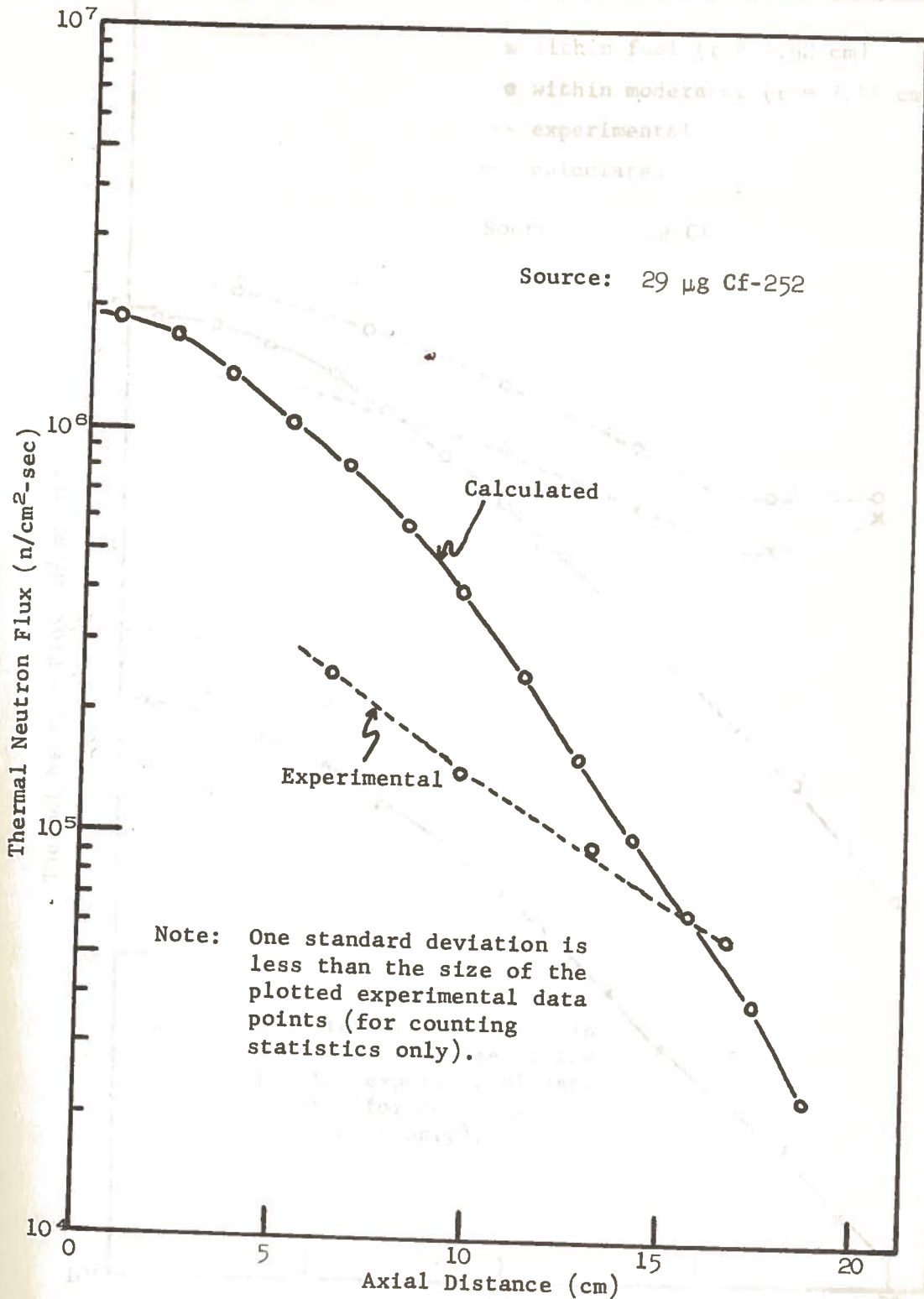
FIGURE 18. Comparison of Experimental and Calculated Thermal (< 0.1 ev) Neutron Fluxes as a Function of Axial Distance for r = 0.
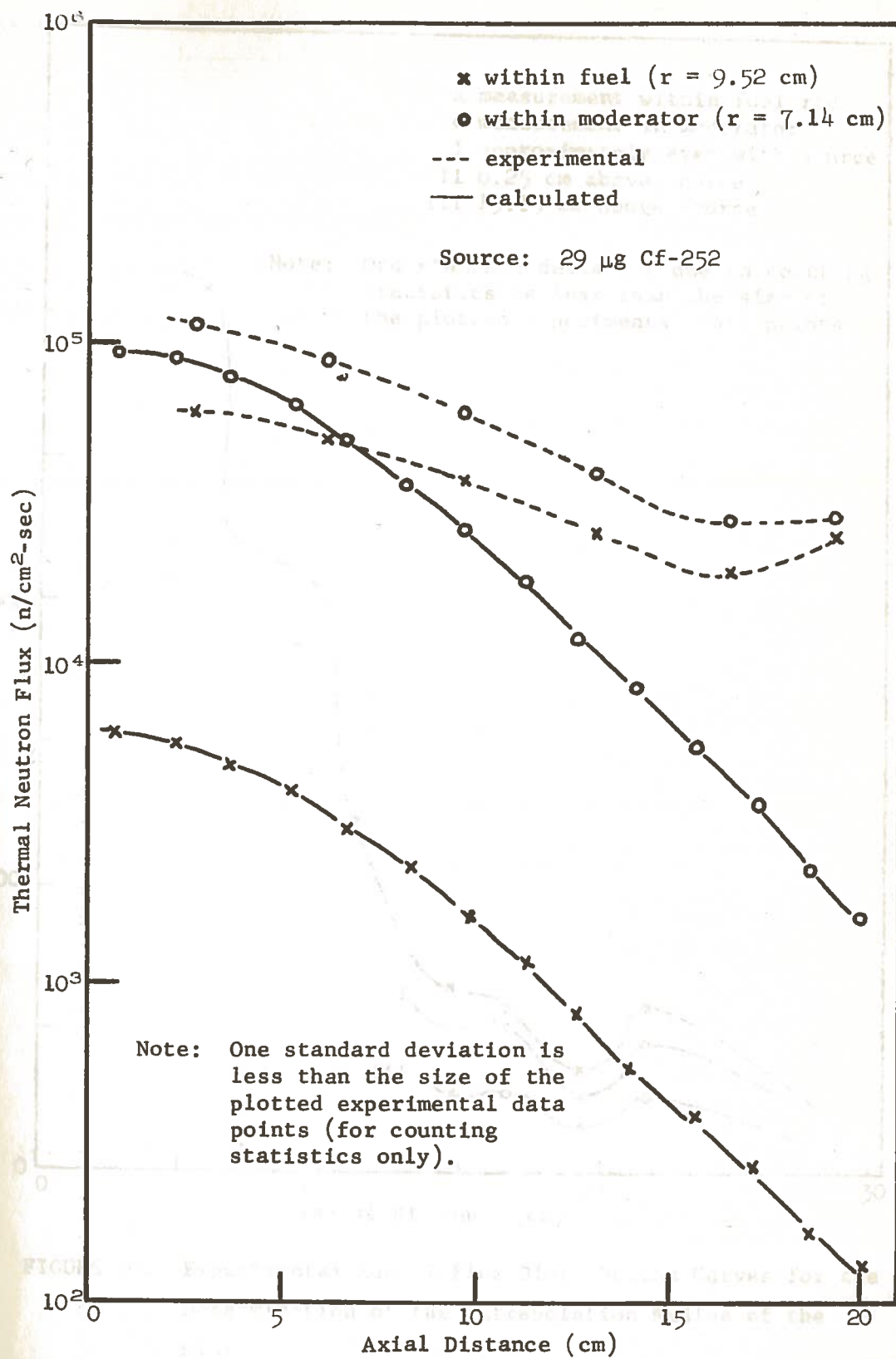
FIGURE 19. Comparison of Experimental and Calculated Thermal (< 0.1 ev) Neutron Fluxes as a Function of Axial Distance in Fuel and in Moderator.

64

x measurement within fuel rod
o measurement in moderator
I approximately even with source
II 6.25 cm above source
III 13.15 cm above source

Note: One standard deviation due to counting statistics is less than the size of the plotted experimental data points.
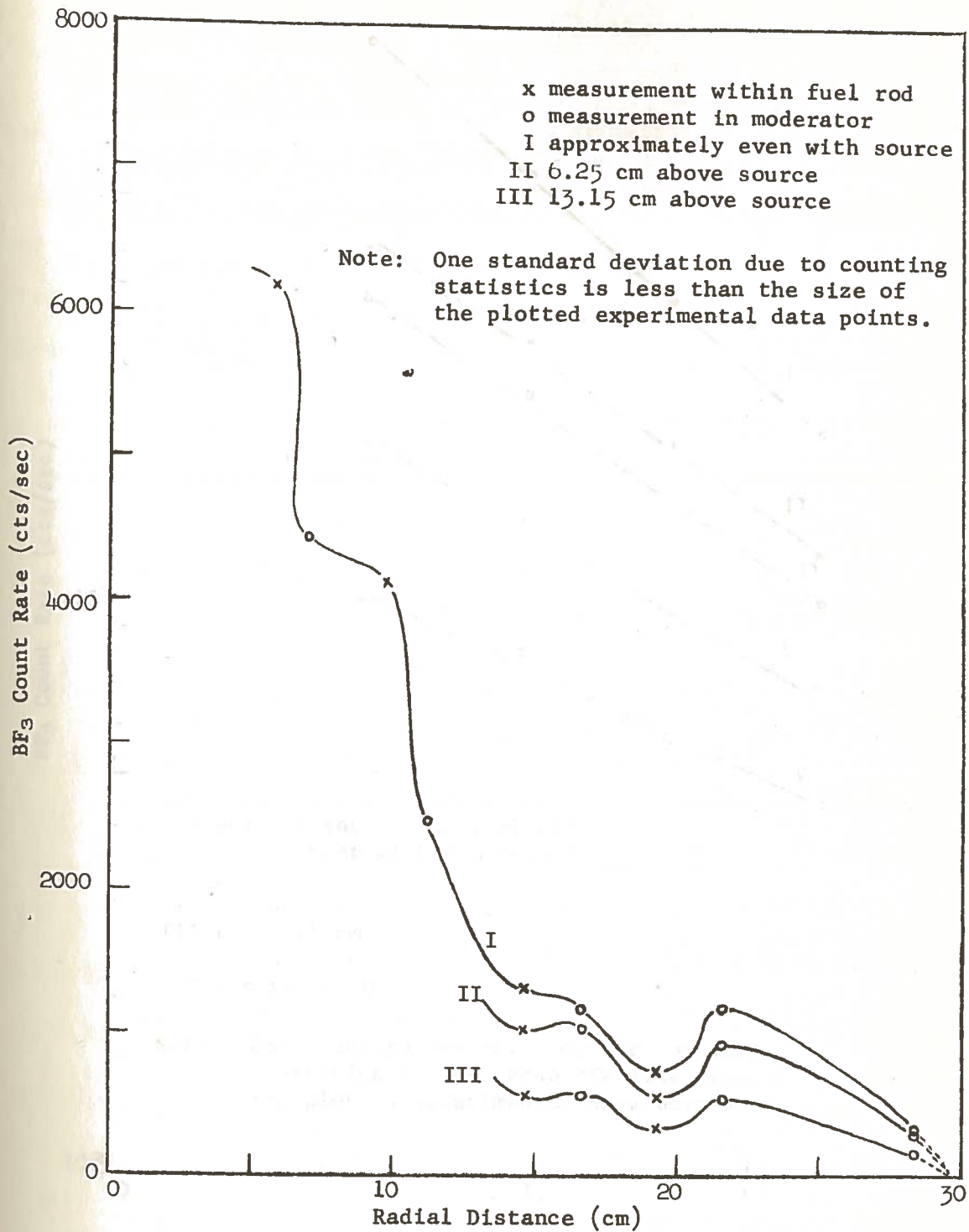
FIGURE 20. Experimental Radial-Flux-Distribution Curves for the Determination of the Extrapolation Radius of the Mini Pile.
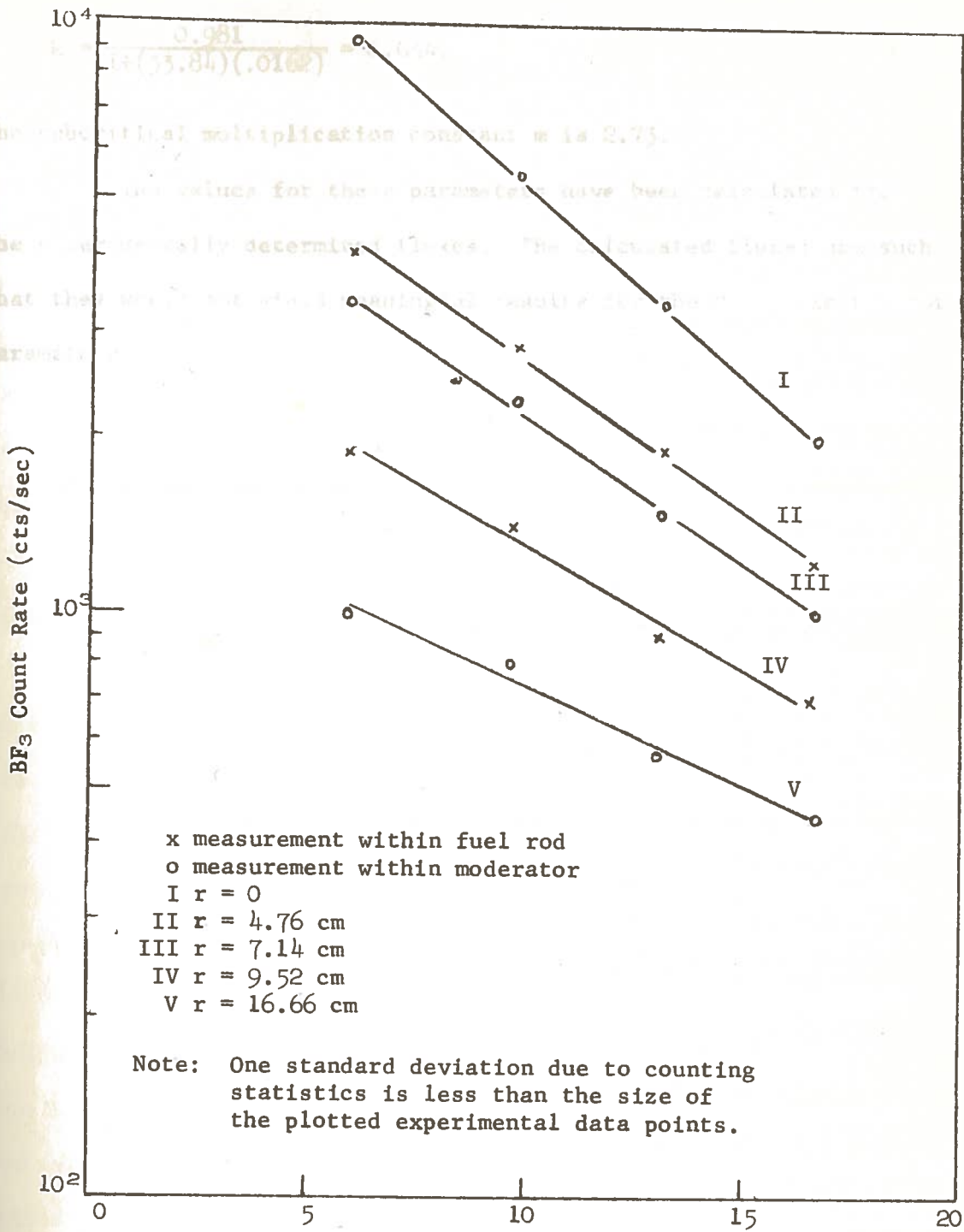
FIGURE 21. Experimental Vertical-Flux-Distribution Curves for
the Determination of the Vertical Buckling of the
Mini Pile.

66

$$k = \frac{0.981}{1+(33.84)(.0162)} = 0.634.$$

The subcritical multiplication constant m is 2.73.

The values for these parameters have been calculated from the experimentally determined fluxes. The calculated fluxes are such that they would not yield meaningful results for the Mini Pile reactor parameters.

CONCLUSIONS AND CRITIQUE

In deriving the discrete ordinates equations, the major approximations consist of the definition of a finite phase space mesh and the subsequent integration of the differential equation over a mesh cell. By choosing a space, angle, and energy mesh sufficiently fine, it is theoretically possible to obtain solutions of the transport equation to any desired degree of accuracy. In practice, however, computer core storage space places a limitation on the degree of accuracy of certain problems.

Besides the limitation of core storage, the user of DOT is restricted to radiation transport problems which can be treated in two-dimensional geometry. The hexagonal array of fuel rods in the Mini Pile require three dimensions for a rigorous description. Due to the symmetry of the system, an attempt was made to treat the problem in two-dimensional r-z geometry.

The fluxes calculated by the DOT code are substantially smaller than the experimentally determined fluxes at large radii. A possible explanation for the large discrepancy between experimental and calculated results is that the hexagonal rings are approximated by cylindrical shells whose surface-to-mass ratio (S/M) is substantially larger than that of the corresponding hexagonal ring. Resonance capture of neutrons while they are slowing down increases as S/M increases, since less uranium is shielded. This increase in resonance capture greatly reduces the amount of neutrons available to cause fission.

The surface area of the uranium in the model becomes increasingly greater than in the actual lattice as the number of fuel rods in a hexagonal ring increase (see Table IV). This would account for some, if not all, of the tremendous decrease in calculated thermal flux at large radii. The discrepancy in the axial direction was not as pronounced, since no fuel cylinders were traversed.

TABLE IV

COMPARISON OF SURFACE AREA OF URANIUM FUEL IN
MODEL AND IN ACTUAL LATTICE

Lattice Ring	Number of Rods	$\left(\dfrac{\text{Actual Area}}{\text{Model Area}}\right)$
1	6	0.32
2	12	0.16
3	18	0.11
4	24	0.08

The large flux depression in the fuel rods for the calculated fluxes is probably due to the explanation above, and also to the lack of moderator within the uranium in the third model.

The determination of the experimental fluxes was accomplished by a BF_3 probe with an active region 5.5 cm in length and 0.6 cm in diameter. The sensitive volume is larger than the mesh blocks. This finite volume makes positioning of the probe at a particular point very difficult, especially if the axial direction is being traversed. For example, the rise in the experimental flux in Figure 19 is probably due to a portion of the BF_3 chamber extending above the rod forest and

detecting neutrons in the reflector. The probe also causes a local flux depression, which makes accurate determination of the flux impossible. A poor voltage plateau (Figure 14) causes variations in the measured count rate.

Another limitation of the DOT code as well as other radiation transport codes is the accuracy of the cross sections. A significant weakness is the knowledge of the cross sections in the resonance region, and the results of the Mini Pile calculations are attributable, at least in part, to the deficiencies in the cross section data[29].

Although the treatment of the Mini Pile problem with the DOT code did not produce results with the desired accuracy, the differences between calculations and measurements can be explained. The Nuclear Science Center now has a multipurpose discrete ordinates transport computer code operable on the LSU IBM 360/65 system. DOT may be used to treat a variety of problems in radiation transport and shielding. The Center also possesses a small subcritical assembly which should prove valuable as an educational and research tool.

REFERENCES

1. A. W. Weinberg and E. P. Wigner, The Physical Theory of Neutron Chain Reactors, (University of Chicago Press, Chicago, 1958).

2. R. V. Meghreblian and D. K. Holmes, Reactor Analysis, (McGraw-Hill Book Company, Inc., New York, 1960).

3. S. Glasstone and M. C. Edlund, The Elements of Nuclear Reactor Theory, (D. Van Nostrand Company, Inc., Princeton, New Jersey, 1960).

4. G. C. Wick, "Über ebene Diffusions probleme", Z. Phys. 121, 702, 1943.

5. S. Chandrasekhar, Astrophys J. 100, 76 (1944).

6. S. Chandrasekhar, Radiative Transfer, Oxford, 1950.

7. B. G. Carlson and G. I. Bell, Solution of the Transport Equation by the S_n Method, "Proceedings of the Second United Nations International Conference on the Peaceful Uses of Atomic Energy, Geneva, 1956", p. 2386, International Atomic Energy Agency, Geneva, 1958.

8. F. R. Mynatt, F. J. Muckenthaler, and P. N. Stevens, "Development of Two-Dimensional Discrete Ordinates Transport Theory for Radiation Shielding", ORNL Report Number CTC-INF-952, Oak Ridge, Tenn., Aug. 11, 1969.

9. G. E. Bell and S. Glasstone, Nuclear Reactor Theory, pp. 216-236 (Van Nostrand Reinhold Company, New York, 1970).

10. F. B. Hildebrand, Introduction to Numerical Analysis, (McGraw-Hill Book Company, New York, 1956).

71

11. K. D. Lathrop, "Discrete Ordinates Quadratures", in A Review of the Discrete Ordinates S_n Method for Radiation Transport Calculations, D. K. Trubey and Betty F. Maskewitz, eds., ORNL, March, 1968.

12. D. Lindstron, "Technical Report and User's Manual/DASH-FORTRAN IV/ Void Tracing and S_n-Monte Carlo Bridging Code", Aerojet Nuclear Systems Company, SRT-TRM01-W393-4C, May, 1970.

13. G. Arfken, Mathematical Methods for Physicists, (Academic Press, New York, 1966).

14. B. G. Carlson, "Numerical Solution of Transient and Steady-State Neutron Transport Problems", USAEC Report LA-2260, October, 1959.

15. B. G. Carlson and K. D. Lathrop, in "Computing Methods in Reactor Physics", H. Greenspan, C. N. Kelber, and D. Okrent, eds., (Gordon and Breach, 1968).

16. B. G. Carlson, Numerical Solution of Neutron Transport Problems, "Proceedings of Symposium in Applied Mathematics, Volume XI", American Mathematics Society, 1961.

17. J. R. Lamarsh, Introduction to Nuclear Reactor Theory, (Addison-Wesley Publishing Company, Inc., Reading, Mass., 1966).

18. F. R. Mynatt, "A User's Manual for DOT", Union Carbide Nuclear Company, K-1694, January, 1967.

19. R. G. Soltesz and R. K. Disney, "User's Manual for the DOT-IIW", Westinghouse Astronuclear Laboratory, WANL-TME-1982, Dec., 1969.

20. Private communication with Michael Gritzner, Neutron Physics Division, Oak Ridge National Laboratory.

21. R. Murray, Nuclear Reactor Physics, (Englewood Cliffs, New Jersey, Prentice-Hall, 1957).

22. J. Barton Hoag, <u>Nuclear</u> <u>Reactor</u> <u>Experiments</u>, (D. Van Nostrand Company, Inc., Princeton, N. J., 1958).

23. F. A. Valente, <u>A</u> <u>Manual</u> <u>of</u> <u>Experiments</u> <u>in</u> <u>Reactor</u> <u>Physics</u>, (The Macmillan Company, New York, 1963).

24. W. H. Shulden, "Design Calculations for a Subcritical Nuclear Reactor with Hollow Natural Uranium Fuel Rods Internally and Externally Moderated with Light Water", M.S. Thesis, The Catholic University of America, June, 1962.

25. R. L. Gorton, "Design of the Louisiana State University Subcritical Nuclear Reactor", M.S. Thesis, Louisiana State University, June, 1960.

26. Private communication with Eugene P. Wigner, consulting professor, LSU.

27. J. C. Courtney, "The Construction and Operational Testing of an Internally and Externally Water Moderated Natural Uranium Subcritical Reactor", M.S. Thesis, The Catholic University of America, June, 1962.

28. "Neutron Activation Foils", prepared by Scientific Staff of Reactor Experiments, Inc.

29. Private communications with Elliot Whitesides, Neutron Physics Division, Oak Ridge National Laboratory.

30. G. E. Hansen and W. H. Roach, "Six and Sixteen Group Cross Sections for Fast and Intermediate Critical Assemblies", LAMS-2543, 1961.

31. Jere P. Nichols, "Design Data for Cf-252 Neutron Source Experiments", Nuclear Applications, Vol. 4, June, 1968.

APPENDIX A

FINAL FORM OF DIFFERENCE EQUATIONS TO BE SOLVED[8]

When the diamond-difference equations, $(2\text{-}37)$-$(2\text{-}41)$, are combined with equation $(2\text{-}35)$, the solution for the flux at the center of a mesh in cylindrical geometry is:

$$
\begin{aligned}
\phi_{G,I,J,D} = (\,|\bar{\mu}_D|\,2\pi\bar{r}_I \Delta z_J
\begin{bmatrix} \phi_{G,i+1,J,D} \\ \text{or} \\ \phi_{G,i,J,D} \end{bmatrix}
+ \, |\bar{\eta}_D|\,2\pi\bar{r}_I \Delta r_I \\[6pt]
\begin{bmatrix} \phi_{G,I,j+1,D} \\ \text{or} \\ \phi_{G,I,j,D} \end{bmatrix}
+ \frac{\Delta z_J}{w_D}\,\bar{\gamma}_N \phi_{G,I,J,n,K} \\[6pt]
+ \tfrac{1}{2} V_{I,J} S'_{G,I,J,D})/(\,|\bar{\mu}_D|\Delta z_J 2\pi\bar{r}_I + \, |\bar{\eta}_D|\,2\pi\bar{r}_I \Delta r_I \\[6pt]
+ \frac{\Delta z_J}{w_D}\,\bar{\gamma}_N + \tfrac{1}{2} V_{I,J}\Sigma_G^T)\,,
\end{aligned}
\qquad (A\text{-}1)
$$

where $\bar{\gamma}_N = \tfrac{1}{2}(\gamma_{n+1} + \gamma_n)$.

$S'_{G,I,J,D}$ includes the fixed source and all scattering sources that have been computed with previous fluxes. The upper term in the first bracket is for $\bar{\mu}_D < 0$ and the upper term in the second bracket for $\bar{\eta}_D < 0$. The lower terms are used for positive values of these direction cosines. The subscripts in the equation have the following significance: "I" and "i" denote the indices in the mesh sweep over r, "J" and "j" over z, "k" and "K" over η, "N" and "n" over ψ, "G" and "g" over the energy E, and D over the quadrature set.

After solving equation (A-1) for the centered flux, the undetermined end point fluxes are given by

$$
\begin{bmatrix} \phi_{G,i,J,D} \\[2mm] \phi_{G,i+1,J,D} \end{bmatrix} = 2\phi_{G,I,J,D} - \begin{bmatrix} \phi_{G,i+1,J,D} \\[2mm] \phi_{G,i,J,D} \end{bmatrix},
$$

$$
\begin{bmatrix} \phi_{G,I,J,D} \\[2mm] \phi_{G,I,j+1,D} \end{bmatrix} = 2\phi_{G,I,J,D} - \begin{bmatrix} \phi_{G,I,j+1,D} \\[2mm] \phi_{G,I,j,D} \end{bmatrix},
$$

and

$$
\phi_{G,I,J,n+1,K} = 2\phi_{G,I,J,D} - \phi_{G,I,J,n,K}.
$$

For a detailed account of rules governing the mesh sweep, the reader is referred to the original work[8].

SUPPLEMENT TO USER'S MANUAL FOR DOT FOR AN IBM 360/65

The following section provides information to a potential user of the DOT-II computer code package from RSIC. To prepare the reader for the suggestions and hints that will be presented, it is urged that he first read "A User's Manual for DOT"[18] and "User's Manual for the DOT-IIW"[19]. The latter publication is extremely useful as a reference even though it describes a slightly modified version of the DOT-II code.

This section consists of information resulting from personal experience in running the code on the LSU computer, private communication with others that are associated with DOT, and some important but subtle points in the DOT manuals that may be overlooked by a potential user.

Changes and Additions to the DOT Code Itself

The following points must be considered before DOT can be made operable on an IBM 360/65:

1. ICLOCK, a timing subroutine in assembler language, should be obtained from RSIC and entered into the DOT program. Otherwise, an unresolved external reference error will occur. A dummy subroutine containing the executable statement "ICLOCK = 0" was attempted at LSU, but failed to solve the problem.

2. In the subroutines WOT and WAT, there are transfer-of-control statements (IF statements) ending DO loops, an intolerable

situation on LSU's G-1 compiler. By using the system utility IEBUPDTE, the statement numbers can be eliminated from the IF statements and placed on CONTINUE cards immediately following the transfer-of-control statements.

3. A WRITE statement in subroutine WWESOL refers to an undefined output unit 51. IEBUPDTE can be used to insert

COMMON NINP,NOUT

after the SUBROUTINE statement, and to change the incorrect WRITE statement to

999 WRITE(NOUT,10)K,ERR.

4. The dimension of the array "A" as specified in MAIN is 90,000. This is much larger than is needed for most problems. The value of LAST in the printout is the amount of variable dimension used, and this value should replace 90,000 in the statement

COMMON/SUPRBU/ISIZE,A(90000).

The value of ISIZE should also be subsequently adjusted on the units assign card.

5. The use of the assembler GRIND instead of the FØRTRAN version is strongly recommended since it decreases computer time by a factor of from two to five[19,20]. The first two comment cards in the assembler version must have a "C" replaced by "*", and one statement in the subroutine must have V(IBCOM) changed to V(IBCOM#) or an unresolved external reference will occur ("#" becomes "=" when printed).

6. Errors in the program that have return severity codes of 4 need not be corrected.

7. The use of hierarchy instead of the overlay structure that accompanied DOT will result in the use of approximately the same amount of CPU time. However, less high-speed core is needed with hierarchy, and faster turn-arounds are possible. The user of the LSU computer is limited to 260K of high-speed core, while some computer facilities allow the user much more.

8. To employ hierarchy, simply omit the overlay cards and insert

    //LKED.SYSIN DD *
    HIARCHY 1,SUPRBU.

Also change the word OVLY to HIAR on the PARM.LKED parameter.

Also change the REGION.GO parameter to

    REGION.GO=(AK,BK)

where A = amount of high speed core needed

and B = amount of low speed core needed.

Job Control Language (JCL) Hints

The following are some suggestions concerning the use of JCL in conjunction with running DOT:

1. The SPACE parameter for SYSLIN, the output from the compiler, must be overridden:

    //FORT.SYSLIN DD SPACE=(800,(400,50),RLSE).

2. The REGION parameter in the GO step defaults to 52K unless overridden. The new value should coincide with the High Water Core Mark (HWCM) on the JOB card.

3. When using the FORTRAN compiler, the PARM parameter should include "NOTERM", which indicates that input/output (I/O) operations are not at a terminal.

4. The DOT source program contains not only FORTRAN, but also the assembler subroutines ICLOCK and GRIND. To compile the program, it is necessary to write an on-line catalogued procedure (PROC) similar to FORTASM, except that the program IEUASM is executed in two separate steps to compile the two assembler subroutines. The PROC, called DOT, is entered in the deck as shown below:

```
(JOB card)
//DOT PROC
(cards for PROC)
//ENDPROC PEND
```

5. In the DD statements assigning storage allocation, the RECFM in the DCB parameters should be VBS.

6. If the program listing of DOT is not desired after every job, include:

```
//SYSPRINT DD DUMMY,SYSOUT=
```

This is appropriate for the LSU system which is operating on Release 20.6.

Suggestions in Technique and Miscellaneous Information

The following suggestions may prove helpful in simplifying data input and minimizing the amount of computer storage and time for solving a problem.

1. It is sometimes possible to simplify a mesh model by using symmetry properties and appropriate reflecting boundary conditions. For example, Figure 22 shows a two-dimensional representation of a cylindrical volume (the cylinder is
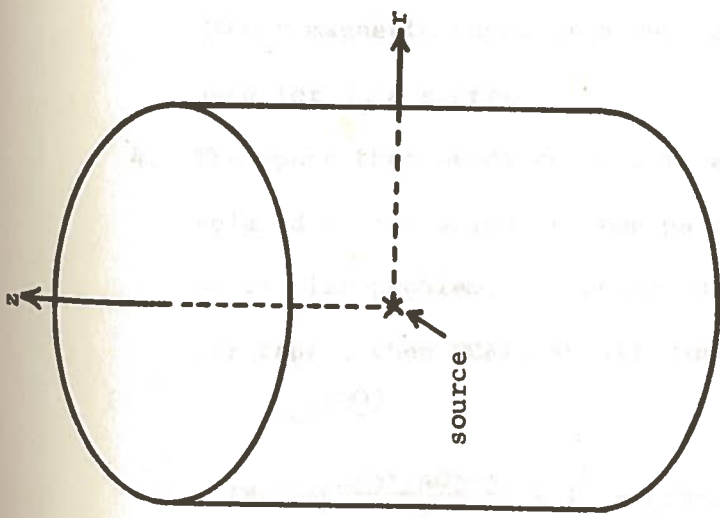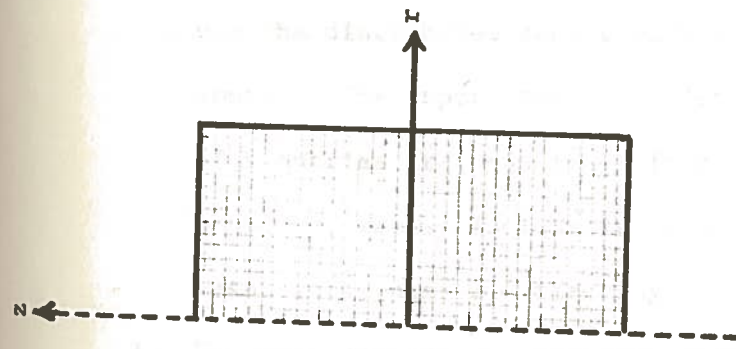
FIGURE 22. Simplification of a Two-Dimensional Mesh Model

generated by rotating the figure about the dotted axis) containing a source at the origin. The simplified mesh model is also shown with the reflective boundaries indicated. The upper portion was chosen as the mesh model because the direction of the mesh sweep during calculations (shown by the arrows) would allow fluxes to be available for reflection at the reflecting boundaries.

2. In a problem with an isotropic source, it is much simpler to use the distributed source option instead of the boundary source. The input data is easier to handle and no angular flux entries are req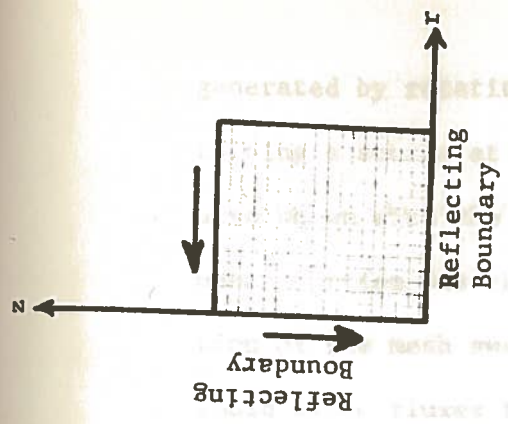uired. If the source is situated at a boundary, merely include it in one or more of the outermost mesh blocks near a reflecting surface.

3. The data storage designations specified on the units assign card are not all required. Those that are not required in a particular problem should have their corresponding parameter values set equal to the value of a unit that is required. Either magnetic tapes or direct access (disk) space can be used for data storage.

4. The space that needs to be allocated to the storage units is related to the value of some parameters associated with a particular problem. If fluxes and moments are out on disk (or tape), then NCR1, NSCRAT, and NFLUX1 must have enough room for[20]

$$IM*JM*\left[\frac{AO3*(AO3+3)}{2} + 1\right] + [IM+JM]*AO4 \text{ words/group.}$$

5. Quadrature weights and direction cosine data are given on the original code package tape.

6. The use of the characters R, I, and F in the data input is strongly recommended to simplify keypunching. A description of their uses can be found on pages 5 and 6 in the DOT-IIW manual[19]. Data can also be entered in exponential (base 10) form.

7. Suggested initial values of the inner iteration parameters S04 and G07 are 8 and 18 respectively[20].

8. The input sequence of the data arrays are as specified in the DOT manual[18]. All other arrays not mentioned follow these in any order.

9. Convergence of inner iterations is vital to insure meaningful solutions; therefore, the use of the pointwise flux convergence criteria (G06≠0.0) is suggested.

10. The rate of convergence of the inner iterations can be accelerated by increasing the value of the convergence criteria, EPS and G06, or by providing a better initial flux estimate. G06 should equal EPS for source calculations.

11. If the normalization factor (S01) in distributed source problems is 1.0, fluxes are in units of n/cm^2-sec-source neutron. If S01 is equal to the distributed source strength in n/sec, fluxes are in units of n/cm^2-sec.

12. The mixed-mode flux calculation option is recommended for most problems.

13. The value of LAMBDA, the ratio of sources, is printed after every other iteration.

14. The mesh spacing requirements specified on page 59 of the DOT-IIW manual[19] are too stringent for most problems. Meshes approximately a centimeter or two in height and width are reasonable except where large flux gradients appear. The disadvantage in going to smaller (and therefore more) meshes to describe a problem is that the resulting computer time increases.

15. When dealing with neutron transport in materials containing low atomic mass numbers such as H_2O, the anisotropic option in DOT must be employed to obtain reasonable results. This is done by using P_ℓ cross sections, where ℓ is the order of scattering. The higher the order of scattering, the more accurate the treatment, but the greater the amount of core and computer time needed. If the order of scattering chosen is i (AO3=i), then the P_o, P_1,...P_i cross sections for that anisotropic material must be entered.

16. The method of handling the input for the cross sections and the use of the mixing table to compute the macroscopic cross sections for a particular problem are described clearly in the DOT-IIW manual[19]. Complications arise when the material in a zone is a mixture or a compound of both isotropic and anisotropic elements. The reader is referred to the mixing table of the Mini Pile problem for the handling of such a situation.

17. For problems involving natural uranium, the cross sections used should be corrected for the resonance integral[29].

18. Recent cross section data are available from RSIC in card form in the format used by DOT. The cards must be translated from BCD to EBCDIC. The LSU system has a data-handling

procedure TOEBCDIC to accomplish this. The P_ℓ cross sections must be multiplied by $2\ell + 1$, which can be done when considering the density of that element in the mixing table. The length of the cross section table (ITL) of these cards is nine.

19. If Hansen and Roach cross sections[30] are used instead, those having $\chi(E)$ spectrum weighting should be used[29].

20. If an "overflow" error message is encountered during the inner iterations while using the point-scaling technique, it is probably caused by an error in either the cross sections or the mixing table resulting in the dominance ratio[19]:

$$\lambda \approx \Sigma gg/\Sigma_t < 1.0$$

being violated.

21. If an "OOC4" error message is encountered, the dimension of "A" is probably too small for that problem.

22. To check the input data for errors, specify DO5=0 for the first run. This will result in a printout of the DOT input.

23. Placing the load module (compiled DOT program) on disk saves over three minutes CPU time every run.

24. To obtain quicker "turn-arounds", the card deck used can be duplicated and two decks submitted independently. Care should be taken in keeping track of what changes are made in each deck.

25. To use the calculated fluxes written out on NFLSV as an initial guess, the unit designations must be switched so that the tape used for NFLSV is designated as NFLUX1. Six areas require consideration when using this method:

(a) The DD statements assignment storage allocations to NFLSV and NFLUX1 must contain the correct disposition (i.e., OLD, KEEP or NEW,KEEP). The DCB parameter is: DCB=(RECFM=VS,LRECL=3516,BLKSIZE=3520).

(b) The designations on the units assign card for NFLSV and NFLUX1 must correspond to the units specified in (a) above.

(c) Enter M07=5 for initial flux guesses from tape.

(d) In problems involving fission or upscatter, D05 may have to be adjusted to a low enough value so that the fluxes will be printed before the specified maximum CPU time is reached. If the outer iterations fail to converge in this alloted time, and if D05 is not sufficiently small, then no fluxes will be written.

(e) NFLUX1 is also used as a scratch tape. The flux guess is read in and subsequently written over and lost. Thus, a flux guess can only be used once unless another copy is available.

26. The pointwise flux convergence option (G06≠0.0) requires convergence in every mesh block before DOT calculates the flux in the lower energy groups. This results in much time being spent on attempting to converge in regions which may be of little interest, such as in corners of the model. The integral iteration test (G06=0.0) can be used for problems that require many outer iterations. Using this option, inner iteration convergence is required over the entire system rather than in the individual meshblocks.

27. The zone of convergence option is available if convergence of some particular zone of interest is desired.

28. The following is an outline of the deck (including JCL) used by the author to run the DOT code on the LSU IBM 360/65:

```
                    (JOB CARD)
                    (SETUP CARD)
                    (ON-LINE PROC NAMED DOT)
//STEP EXEC DOT,PARM.FORT=`MAP,OPT=0,NOTERM',
//      TIME=19,REGION.ASM1=150K,
//      PARM.LKED=`XREF,LET,LIST,HIAR',
//      REGION.GO=(200K,250K),
//      PARM.GO=`IO=-1,ID=-1,EO=-1,EV=-1,FD=-1'
//FORT.SYSLIN DD SPACE=(800,(400,50),RLSE)
//FORT.SYSIN DD DSN=D7011.P40010.LANDRY.DOTNOG,
//      UNIT=2314,VOL=SER=LSU007,DISP=(OLD,KEEP),
//      DCB=(RECFM=FB,LRECL=80,BLKSIZE=7280)
//ASM1.SYSIN DD UNIT=2314,VOL=SER=LSU007,
//      DSN=D7011.P40010.LANDRY.ASSGND,
//      DISP=(OLD,KEEP),DCB=(RECFM=FB,LRECL=80,BLKSIZE=7280)
//ASM2.SYSIN DD *
                    (ICLOCK CARDS)
//LKED.SYSIN DD *
 HIARCHY 1,SUPRBU
//GO.FT10F001 DD UNIT=SYSDA,SPACE=(TRK,(800,100),RLSE),
//      DCB=(RECFM=VBS,LRECL=3516,BLKSIZE=3520)
//GO.FT11F001 DD UNIT=SYSDA,SPACE=(TRK,(800,100),RLSE),
//      DCB=(RECFM=VBS,LRECL=3516,BLKSIZE=3520)
//GO.FT12F001 DD UNIT=TAPE,
//      DSNAME=EDTWO.GUESS.TWO,VOL=SER=T1903,
//      DCB=(RECFM=VS,LRECL=3516,BLKSIZE=3520),
//      DISP=(OLD,KEEP),LABEL=(1,SL)
//GO.FT14F001 DD UNIT=TAPE,
//      DSNAME=FLUX.EDTWO,VOL=SER=T1267,
```

```
//         DCB=(RECFM=VS,LRECL=3516,BLKSIZE=3520),
//         DISP=(NEW,KEEP),LABEL=(2,SL)
//GO.SYSIN DD *
```

(DATA CARDS)

```
//
```

APPENDIX C

DATA INPUT TO DOT FOR THE MINIPILE PROBLEM

One of the useful features of the DOT code is the simplicity with which one can alter the problem under consideration. Three different models were used to describe the Mini Pile problem, and the modification of the input to handle each was a relatively simple task. Tables V and VI contain sample input parameters and data arrays for the Mini Pile problem. Some of these values may be different when using special techniques, such as an initial flux guess from tape.

Since the DOT code handles only two-dimensional problems, the hexagonal lattice structure was approximated by concentric, cylindrical shells of natural uranium separated by water. The first model consisted of uranium shells of thickness equal to that of the rods. These shells were located at the radial position corresponding to the hexagonal array that they represented.

The second model was constructed to provide a more realistic representation by considering the ratio of the fuel to moderator in the shell, and utilizing an effective thickness of uranium (see Figure 23). Using the notation in Figure 23, the areas of the entire annular ring, of the uranium, and of the water are:

$$A_{r_1 \to r_3} = \pi(r_3^2 - r_1^2) \tag{C-1}$$

$$A_U = n\pi(r_0^2 - r_4^2) \tag{C-2}$$

$$A_{H_2O} = A_{r_1 \to r_3} - A_u \tag{C-3}$$

where n = number of fuel rods.

88

TABLE V

INPUT PARAMETERS FOR MINI PILE PROBLEM

ISIZE = 31160	A01 = 1	IM = 30	B01 = 1
NINP = 5	A02 = 0	JM = 8	B02 = 0
NCR1 = 10	A03 = 1	IO4 = 0	B03 = 0
NSCRAT = 11	A04 = 16	EV = 0.0	B04 = 1
NBSO = 10	IGE = 1	EVM = 0.0	M07 = 0
NPSO = 10	IZM = 2	EPS = .1	MODE = 1
NFLUX1 = 12			
NAFT = 10			
NFLSV = 14			

MT = 8	S02 = 0	S01 = 6.8×10^7
M01 = 8	S03 = 0.0	NACT = 4
MCR = 5	IGM = 16	M06 = 3
MTP = 0	IHT = 3	S04 = 8
IZ = 0	IHS = 4	D05 = 10
JZ = 0	ITL = 9	G07 = 18

TMAX = 20	IAFT = 0	ITI = 0
G06 = .1	IZC = 0	IP1 = 2
LAL = 0.0	IMG = 0	IP2 = 0
LAH = 0.0	ISC = 0	IP3 = 0
POD = 0.0	IS2 = 0	IP4 = 0
EPSA = .001	IS3 = 0	IP5 = 0

TABLE VI

DATA ARRAYS FOR MINIPILE PROBLEM

| Array	Number of Entries	Description of Entries
7*	32	Direction cosines: 16 μ's, 16 η's
6*	16	Quadrature weights
14*	720	Cross sections from cards: $H(P_0)$, $H(P_1)$, Oxygen, U-235, U-238
3-17*	16, 30, 8	Volume distributed fixed source: Cf-252 spectrum by groups; one 1.0 entry followed by twenty-nine 0.0's; one 1.0 entry followed by seven 0.0's
3*	16	Initial flux: all entries are 0.0
4*	31	Radial interval boundaries
2*	9	Axial interval boundaries
8$	240	Zone numbers by interval
9$	2	Material numbers by zone: -6 and 8
1*	16	Fission spectrum
5*	16	Velocities: all entries are 1.0
10$	8	Mixing table, sums: 6, 7, 6, 7, 6, 8, 8, 8
11$	8	Mixing table, components: 0, 0, 1, 2, 3, 0, 4, 5
12*	8	Mixing table, atomic densities: 0.0, 0.0, $\rho(H)$, $\rho(H)$x3, $\rho(0)$, 0.0, $\rho(U\text{-}235)$, $\rho(U\text{-}238)$
19$	4	Material numbers for activity print: 5, 6, 6, 6
20$	4	Cross section table position for activity print: 1, 1, 2, 3

Ratio of U to H₂O in this region is the same as in the actual lattice
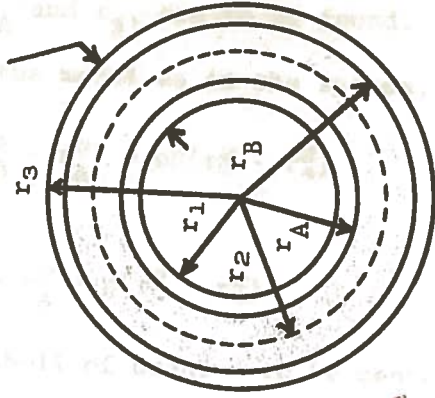
Second Model
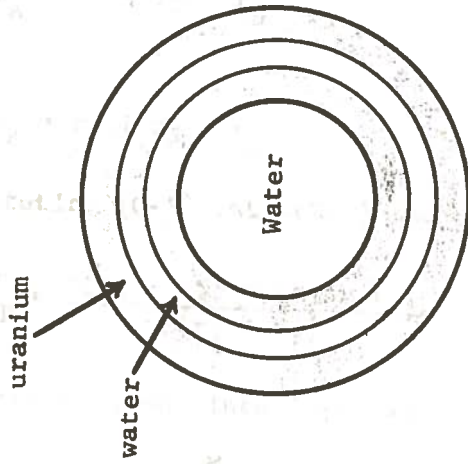
First Model
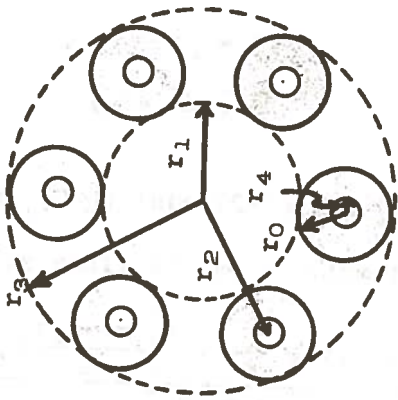
Actual Lattice

FIGURE 23. Lattice Models Used in the DOT Mini Pile Problem

91

The radii r_0, r_1, r_1, r_2, and r_4 are known. The effective radii, r_A and r_B, are to be found. If the area of uranium is to be the same in the model as in the system,

$$\pi(r_B^2 - r_A^2) = n\pi(r_0^2 - r_4^2)$$

or

$$r_B^2 - r_A^2 = n(r_0^2 - r_4^2) \tag{C-4}$$

For the shell of uranium to be centered,

$$r_3 - r_B = r_A - r_1$$

or

$$r_A = r_1 + r_3 - r_B \tag{C-5}$$

and

$$r_B = r_1 + r_3 - r_A \tag{C-6}$$

Substituting (C-5) into (C-4) and solving for r_B gives:

$$r_B = \frac{n(r_0^2 - r_4^2) + (r_1 + r_3)^2}{2(r_1 + r_3)} \tag{C-7}$$

Substituting (C-6) into (C-4) and solving for r_A gives:

$$r_A = \frac{(r_1 + r_3)^2 - n(r_0^2 - r_4^2)}{2(r_1 + r_3)} \tag{C-8}$$

From Figure   , $r_3 - r_1 = 2r_0$

or

$$r_0 = \frac{r_3 - r_1}{2} \tag{C-9}$$

Substituting (C-9) into (C-7) and (C-8) yields general expressions for the effective radii of the uranium fuel shells:

$$r_B = \frac{n[(\frac{r_3 - r_1}{2})^2 - r_4^2] + (r_1 + r_3)^2}{2(r_1 + r_3)} \tag{C-10}$$

$$r_A = \frac{(r_1 + r_3)^2 - n[(\frac{r_3 - r_1}{2})^2 - r_4^2]}{2(r_1 + r_3)} \qquad (C\text{-}11)$$

Table V contains the values of the effective radii for the second model of the Mini Pile.

TABLE VII

VALUES OF EFFECTIVE RADII FOR CYLINDRICAL URANIUM SHELLS

Number of Fuel Rods n	r_A (cm)	r_B (cm)
6	4.16	5.36
12	8.92	10.12
18	13.67	14.87
24	18.44	19.64

The third model representing the Mini Pile is identical to the second except that more axial mesh blocks were considered. The second model consisted of 8 axial mesh blocks, 3.45 cm in height. To reduce the size of these, 18 mesh blocks were considered, each approximately 1.5 cm in height.

VITA

Edward J. Landry was born on August 2, 1947, in Baton Rouge, Louisiana. He attended Redemptorist High School in Baton Rouge, and graduated in 1965.

In 1965 he entered Louisiana State University and graduated in January of 1970 with a B.S. in physics. He subsequently entered graduate school in the same field and held a teaching assistantship in the LSU Physics Department.

In September of 1970, he decided to pursue graduate studies in nuclear engineering at LSU. At that time he received a graduate assistantship in the Nuclear Science Center. During the past year, he has been involved with a research project for the determination of cement content through nuclear techniques.

On May 26, 1972, he received his commission as a Second Lieutenant in the United States Air Force. He has been assigned to Satellite and Missle Systems Organization (SAMSO), Los Angeles, California.